TECHNICAL REPORT
https://doi.org/10.1038/s41590-019-0544-5
nature immunology

TCR sequencing paired with massively parallel 3′ RNA-seq reveals clonotypic T cell signatures

Ang A. Tu[1,2,10], Todd M. Gierahn[1,10], Brinda Monian[1,3], Duncan M. Morgan[1,3], Naveen K. Mehta[1,2], Bert Ruiter[4,5], Wayne G. Shreffler[4,5,6], Alex K. Shalek[1,7,8,9*] and J. Christopher Love[1,3,8,9*]

High-throughput 3′ single-cell RNA-sequencing (scRNA-seq) allows cost-effective, detailed characterization of individual immune cells from tissues. Current techniques, however, are limited in their ability to elucidate essential immune cell features, including variable sequences of T cell antigen receptors (TCRs) that confer antigen specificity. Here, we present a strategy that enables simultaneous analysis of TCR sequences and corresponding full transcriptomes from 3′-barcoded scRNA-seq samples. This approach is compatible with common 3′ scRNA-seq methods, and adaptable to processed samples post hoc. We applied the technique to identify transcriptional signatures associated with T cells sharing common TCRs from immunized mice and from patients with food allergy. We observed preferential phenotypes among subsets of expanded clonotypes, including type 2 helper CD4$^+$ T cell (T_H2) states associated with food allergy. These results demonstrate the utility of our method when studying diseases in which clonotype-driven responses are critical to understanding the underlying biology.

Antigen-specific T cells play key roles in a number of diseases, including autoimmune disorders and cancer[1–3]. Assessing the phenotypes and functions of these cells is essential to both understanding underlying disease biology and designing new therapeutic modalities[4,5]. To study antigen-specific T cells comprehensively, two sequencing-based approaches have emerged: bulk genomic sequencing of *TCR* gene repertoires to assess clonal diversity and RNA-sequencing (RNA-seq) to reveal phenotypic attributes. The TCR recognizes antigenic peptides bound in major histocompatibility complex (MHC) receptors and mediates CD3-dependent signaling on cognate recognition; sequencing of the *TCR* repertoire thus can highlight clonotypic diversity and the dynamics of antigen-dependent responses associated with disease, such as clonal expansion or selection[2,6,7]. RNA-seq, in contrast, can reveal novel states and functions of disease-relevant T cells through unique patterns of gene expression, albeit without determination of whether those cells are recognizing common antigens[8–10].

Coupling these two types of data is of great interest for modeling the dynamics of T cell responses and isolating those cells that are most relevant to disease states[11–13]. Currently, the preferred method for linking these measures relies on sorting single T cells into multi-well plates by flow cytometry, performing full-length scRNA-seq and then reconstructing the sequences of rearranged *TCRα* and *TCRβ* genes. This strategy is limited in throughput (~10 to 1,000 cells) by cost, labor and time[6,14,15]. Recently developed high-throughput scRNA-seq methods can profile the transcriptomes of 10^3–10^5 single cells at once, but accomplish this task by first barcoding messenger RNAs on their 3′ ends during reverse transcription, followed by quantification of gene expression by sequencing only those 3′ ends[16–18]. While sufficient to enumerate mRNA abundances, this process hinders precise, direct sequencing of recombined *TCR* genes because the variable regions of those transcripts—particularly the complementarity-determining region 3 (*CDR3*) regions closer to the 5′ end of those mRNAs—are not captured efficiently by 3′ library preparation and sequencing protocols[9]. Primer-based approaches that target constant regions of the *TCR* transcripts to directly enrich CDR3 sequences eliminate reverse transcription-appended cellular barcodes and unique molecular identifiers (UMIs) positioned on the 3′ ends of transcripts during amplification, and thus obscure the single-cell resolution of the data.

New approaches have emerged to determine clonotypes from high-throughput 3′ or 5′ scRNA-seq libraries. These typically rely on specialized RNA capture reagents (for example, the customized *TCR* transcript capture beads of DART-seq or specific kits for InDrop, Dolomite and 10X), limiting their adoption and application to previously archived samples. Some also require combinations of different sequencing technologies (for example, Illumina and Nanopore in RAGE-seq), complicating their implementation[11,19–23]. Methods that allow for cost-efficient and simple recovery of *TCR* sequences from 3′ scRNA-seq libraries would enable the study of clonotypic T cell responses with confidence.

Results

***TCR CDR3* sequences recovered via targeted sequencing.** Here, we report a simple process to sequence concomitantly both the transcriptome and *TCRα* and *TCRβ* sequences of T cells from a single sequencing library generated using a massively parallel 3′ scRNA-seq platform, such as Seq-Well or Drop-seq (Fig. 1). Our approach both overcomes the 3′ bias and maintains the single-cell resolution in the sequencing library introduced by these platforms (Supplementary Fig. 1a,b). In our approach, a 3′-barcoded whole-transcriptome amplification (WTA) is performed using standard protocols for Seq-Well or Drop-seq[16,18,24]. Next, one fraction of the amplified product is used to generate a 3′ scRNA-seq library

[1]Koch Institute for Integrative Cancer Research, MIT, Cambridge, MA, USA. [2]Department of Biological Engineering, MIT, Cambridge, MA, USA. [3]Department of Chemical Engineering, MIT, Cambridge, MA, USA. [4]Center for Immunology & Inflammatory Diseases, Massachusetts General Hospital, Boston, MA, USA. [5]Harvard Medical School, Boston, MA, USA. [6]Food Allergy Center, Massachusetts General Hospital, Boston, MA, USA. [7]Institute for Medical Engineering & Science and Department of Chemistry, MIT, Cambridge, MA, USA. [8]Broad Institute of MIT and Harvard, Cambridge, MA, USA. [9]Ragon Institute of MGH, MIT and Harvard, Cambridge, MA, USA. [10]These authors contributed equally: Ang A. Tu, Todd M. Gierahn.
*e-mail: shalek@mit.edu; clove@mit.edu

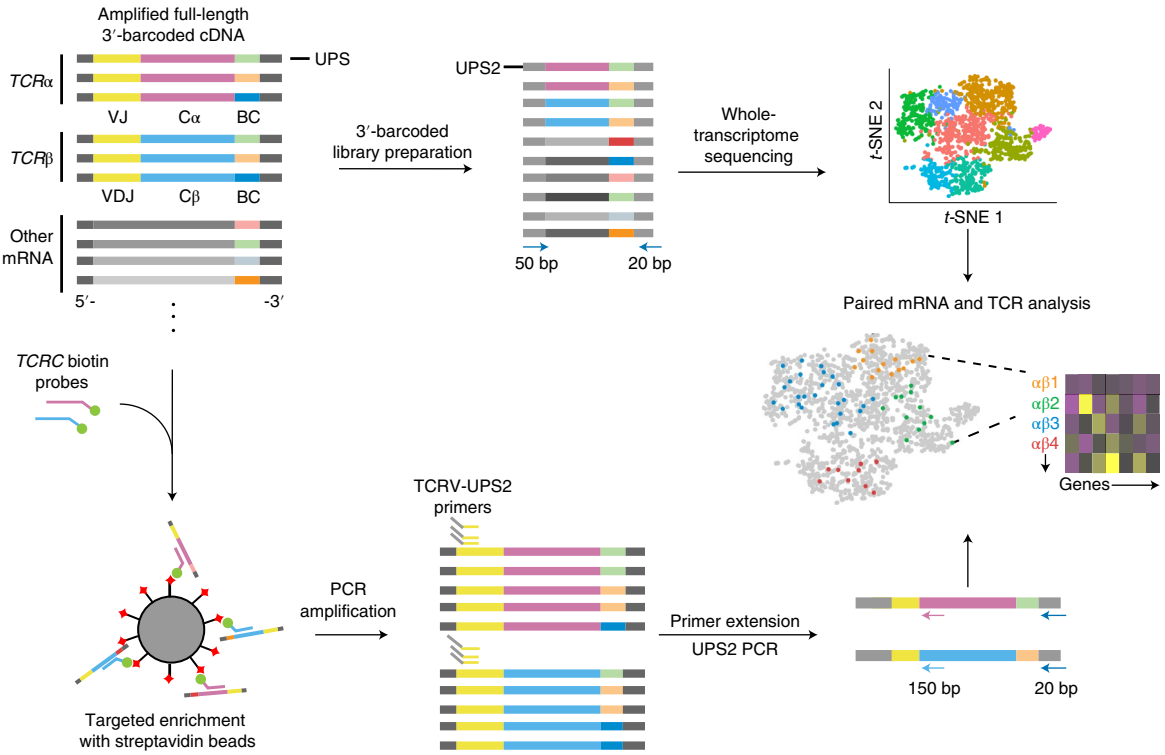

Fig. 1 | Strategy for TCR recovery from 3′-barcoded single-cell sequencing libraries. Barcoded complementary DNA libraries (WTA products) including *TCRα* and *TCRβ* transcripts, in addition to other transcripts (top). Fragmentation and selective amplification of cDNA results in the sequencing library used for transcriptomic sequencing, and analyzed via 3′ gene mapping as previously described[18]. *TCR* enrichment of the same cDNA library through affinity capture with biotinylated oligonucleotides results in amplified products enriched in *TCRα* and *TCRβ* transcripts. The sequencing library is made by primer extension with V-region primer sets, followed by PCR amplification using the UPS2 handles (bottom). The *CDR3* region is sequenced using Illumina MiSeq with custom sequencing primers, and merged with the transcriptomic data on the basis of single-cell barcodes (BC).

to quantify single-cell mRNA expression levels in individual cells; another fraction is used to perform direct single-cell sequencing of *TCRα* and *TCRβ* transcripts. For the latter, *TCRα* and *TCRβ* transcripts contained within amplified 3′-barcoded WTA products are first enriched by affinity capture using biotinylated oligonucleotide probes targeting sequences that encode the TCR constant regions, and they are then re-amplified with the same universal primer site (UPS) used in the original WTA (Supplementary Tables 1 and 2). This step yields up to a 10^4-fold enrichment of TCR-encoding fragments, as determined by quantitative PCR (qPCR) (Supplementary Fig. 1c). Next, the amplified pool is selectively modified by primer extension using a set of oligonucleotides comprising a shared 5′ second universal primer site (UPS2) linked to regions specific for each *TCRα* or *TCRβ* variable (V) region (Supplementary Table 3). The modified products are then further amplified with primers specific for UPS2 and an extended version of the original UPS, which is only present on the 3′ end of the library. This final amplification adds flanking regions of oligonucleotides for sequencing to the *TCR*-enriched library (Supplementary Table 2). The combination of targeted enrichment and primer extension produces a size-defined, *CDR3*-enriched library that does not require additional fragmentation before short-read sequencing (for example, Illumina). The resulting library can then be sequenced using custom primers targeting the constant regions of the *TCR* genes to directly recover the *CDR3* region (Fig. 1 and Supplementary Table 4). This approach produces high-quality coverage of the *CDR3* region as well as the original cellular and molecular identifiers appended during WTA, making it possible to match *TCR* sequences computationally with the corresponding whole-transcriptome profiles determined using traditional 3′ scRNA-seq (Supplementary Fig. 1d).

Paired *Tcra* and *Tcrb* sequences recovered from OT-I T cells. To test the sensitivity of our approach, we enriched *TCR* transcripts from Seq-Well WTA products derived from mouse splenic T cells spiked with T cells from an OT-I transgenic *Rag1*$^{+/+}$*Rag2*$^{+/+}$ mouse (0.01–10%). We recovered *Tcra* (25 ± 3%) and *Tcrb* (65 ± 4%) *CDR3* sequences from cells detected in our whole-transcriptome data ($n = 4$ samples). Both chains were recovered for 20 ± 3% of cells—similar to the predicted rate of recovery, assuming the capture of each transcript is an independent event (16 ± 7%; Supplementary Fig. 2a). Mapped *Tcr* sequences coincided with expression of T cell markers, such as *Cd3e* (Supplementary Fig. 2b). Sequences sharing the same UMI also had a high degree of sequence consensus (Supplementary Fig. 2c; Methods). The proportion of OT-I *CDR3* sequences recovered in each sample was consistent with expectations (Fig. 2a). Cells with an OT-I *Tcra* chain almost exclusively matched to the expected OT-I *Tcrb* chain (97.7%; 33/34 cells); cells with OT-I *Tcrb* chains, meanwhile, primarily matched with the expected OT-I *Tcra* chain (70.5%; 33/45), although not exclusively (Fig. 2b). These results are similar to previous studies, wherein *Rag1*$^{+/+}$*Rag2*$^{+/+}$ OT-I T cells were observed to produce functional TCRα chains, in addition to the OT-I TCRα chain[25].

***CDR3* recovery correlates with abundance of *TCR* transcripts.** We next assessed the relationship between the fraction of cells expressing *TCR* transcripts in their whole-transcriptome data (on the basis of *TCR* constant-region mapping) and the percentage of *CDR3* sequences recovered from the same cells (Fig. 2c). We observed a high correlation: cells with more copies of *TCR* transcripts in their whole-transcriptome data yielded higher rates of *CDR3* recovery from the *TCR*-targeted libraries (*Tcra*: $r_s = 1$, $n = 5$, $P = 0.017$

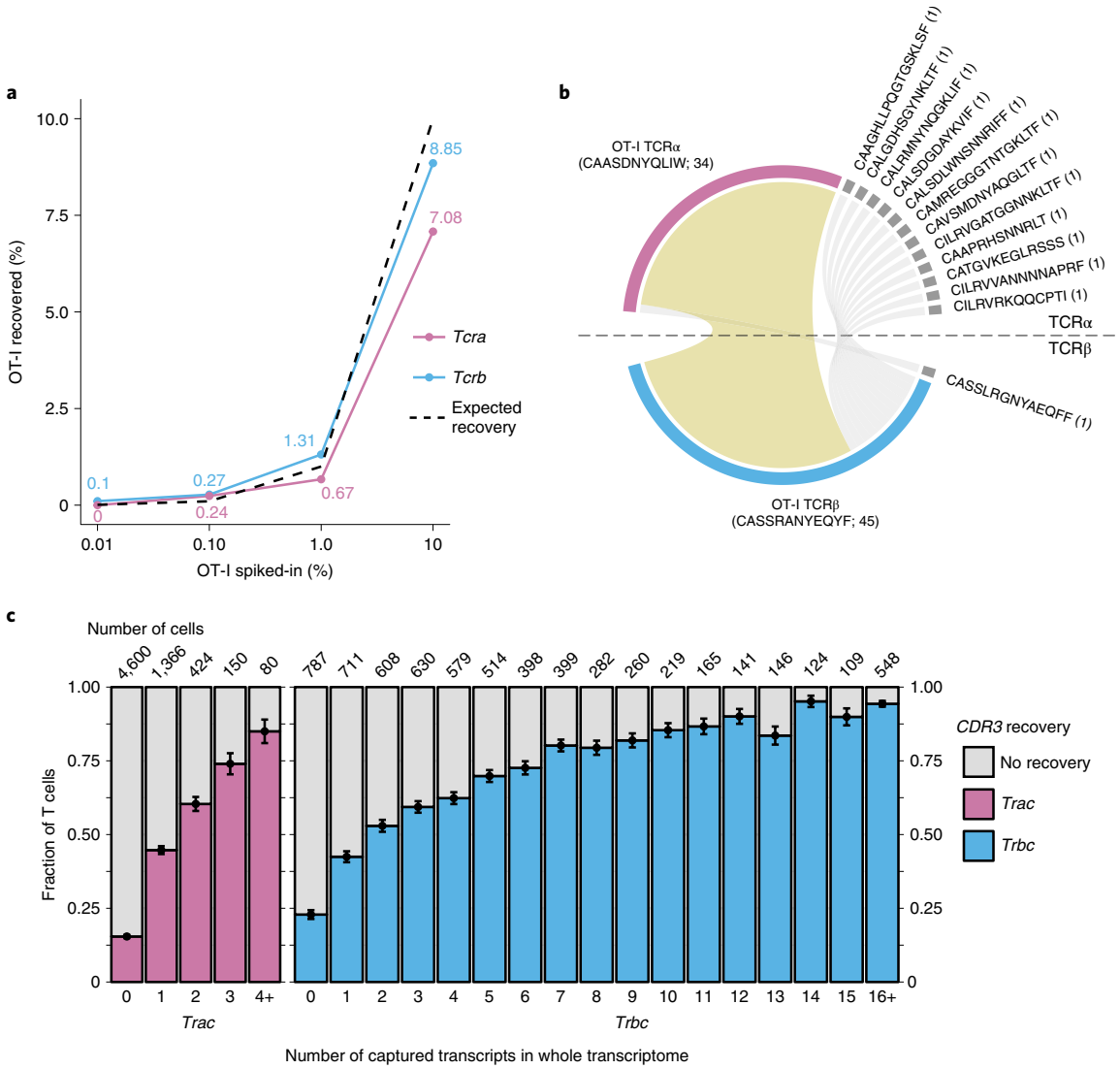

Fig. 2 | Recovery of OT-I *Tcra* and *Tcrb CDR3* sequences. a, Proportions of recovered OT-I *Tcra* and *Tcrb* sequences from murine samples spiked-in with 10%, 1%, 0.1% and 0.01% OT-I *Rag1*$^{+/+}$*Rag2*$^{+/+}$ T cells. Dashed line indicates the expected recovered proportions. **b**, Pairing of recovered OT-I *Tcra* and *Tcrb* chains from cells in all spiked-in libraries with either OT-I *Tcra* or *Tcrb* chain sequences. Number of detected cells indicated in parentheses. Khaki shading indicates pairing of OT-I *Tcra* and *Tcrb* sequences from recovered cells. **c**, Proportion of T cells with successful *CDR3* recovery (*y* axis) as a function of the constant-region mapping via scRNA-seq by Seq-Well (*x* axis). Numbers of cells with the corresponding number of *TCR* constant-region transcripts within their 3′ scRNA-seq data are indicated above the respective column. Error bars indicate standard deviation of estimated binomial distribution.

by Spearman; *Tcrb*: $r_s = 1$, $n = 15$, $P < 10^{-6}$ by Spearman). Overall, excluding classified T cells with no detected *TCR* genes in their transcriptomic data, we recovered *CDR3β* from an average of 70 ± 4% of cells, and *CDR3α* from 52 ± 3%, resulting in combined pairings of *Tcra* and *Tcrb* sequences for 40 ± 4% of T cells (Supplementary Fig. 2a). Finally, we investigated the reproducibility of our approach by comparing technical replicates of the *TCR*-targeted libraries produced from the same starting WTA material. Across replicates, 94% of detected cellular barcodes were the same, and 99.7% of detected shared transcripts (12,849 out of 12,883) resulted in identical assignment of clonotypes (Supplementary Table 5). Taken together, our results show that the method allows consistent and reproducible recovery of *CDR3* sequences with high yields.

***TCR* recovery reveals clonal expansion in immunized mice.** Antigen-specific T cells are often enumerated by flow cytometry using tetrameric reagents comprising known antigenic peptides bound to recombinant MHC molecules. The same peptide–MHC complex, however, can select multiple T cell clonotypes[26]. This intrinsic multiplicity can obscure the underlying relationships between phenotypic states and associated clonotypes. We sought to resolve the clonotypic diversity of tetramer-sorted T cells by applying our approach to murine T cells specific to a canonical envelope antigen (E7) from human papilloma virus (HPV16). After immunization and challenge, splenocytes were collected from the mice. Half of the splenocytes were stimulated ex vivo with E7 antigen for 6 h, and half of the cells were not (Methods). E7 tetramer^{+}CD8^{+} T cells were then sorted from both groups of splenocytes (Supplementary Fig. 3a). These cells were prepared for scRNA-seq using Seq-Well, and their TCR *CDR3* sequences were recovered (Supplementary Fig. 3b). In total, 14,424 cells from four mice were included in the study. We found a diverse set of clonal, expanded T cells within the tetramer-sorted populations isolated from individual animals (Supplementary Table 6). For each animal, the 20 most expanded *Tcrb* clones accounted for 69–89% of recovered T cells (mean = 908 ± 332 cells; Supplementary Fig. 3c). Between 77% and

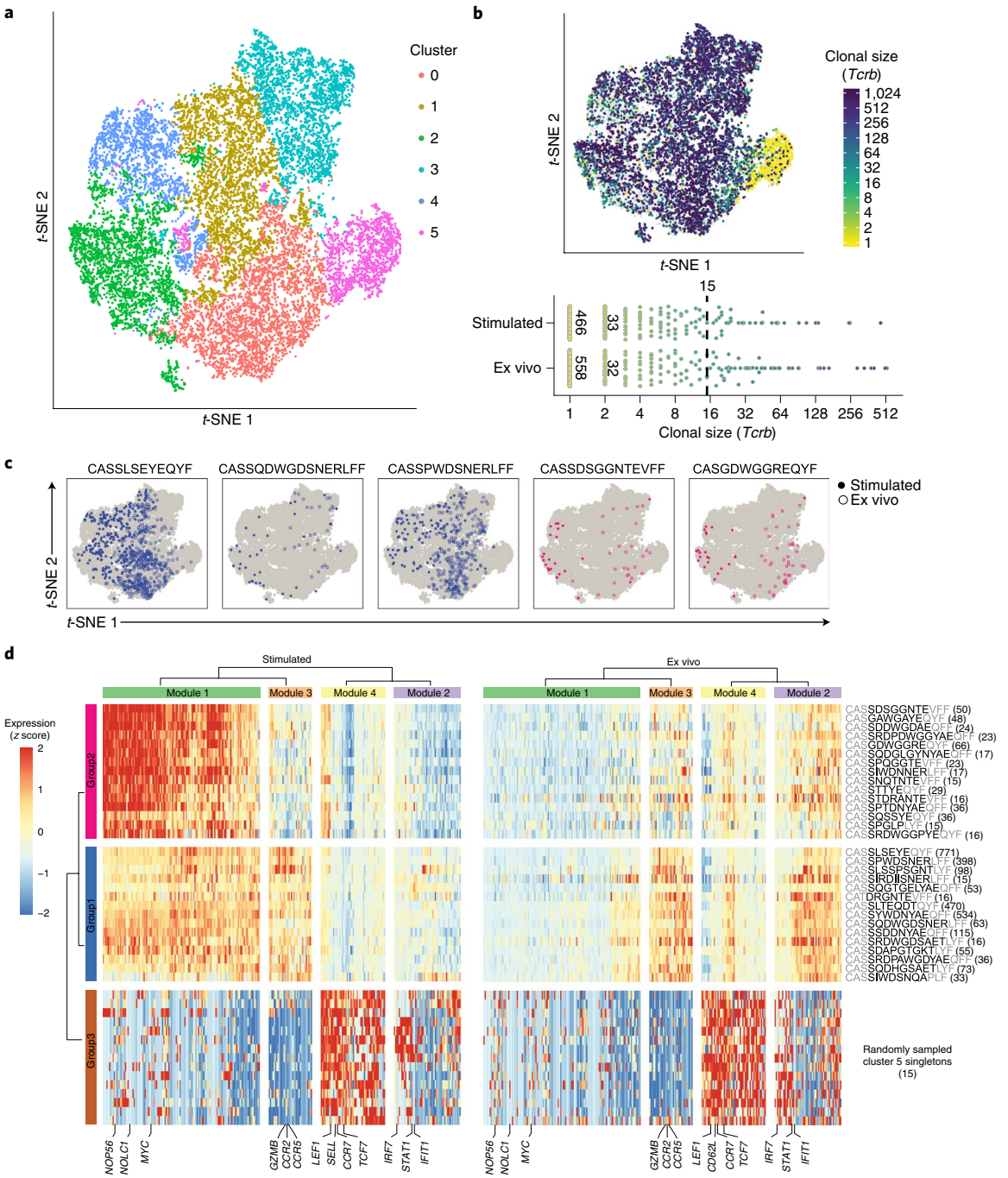

Fig. 3 | scRNA-seq and TCR analysis of HPV-E7-immunized mice. a, *t*-SNE visualization of all cells colored by computationally determined clusters on the basis of transcriptomic data ($n = 14{,}424$ cells). **b**, Clonal size of *Tcrb* chain mapped on *t*-SNE visualization of scRNA-seq results. Cells are colored by the clonal size of their detected *Tcrb* clonotype (top). Clonal size is defined as the number of cells that share the particular clonotype. Distribution of differentially expanded clonotypes between the stimulated and ex vivo conditions (bottom). Each colored circle indicates a unique clonotype. **c**, Example mappings of selected clonotypes from groups 1 (blue) and 2 (magenta) shown in **d** on *t*-SNE visualization of all cells. **d**, Heat maps of differentially expressed genes amongst the expanded clonotypes (≥15 cells) and 15 randomly sampled nonexpanded cells (singletons) from cluster 5 (see **a**) between the ex vivo and antigen-stimulated conditions. Gene expression represents scaled averages within cells of the same clonotype across the two conditions. Number of cells shown in parentheses. Data represent combined data from four independent experiments of four mice total (**a**–**d**).

90% of the recovered T cells had clonal *Tcrb* chains. In total, over 900 unique *Tcra* and 1,200 unique *Tcrb* clonotypes were detected.

We next analyzed the clonality of these cells with respect to their whole transcriptomes (Fig. 3a,b and Supplementary Fig. 3d,e). The majority of stimulated cells were transcriptionally distinct from unstimulated cells isolated directly ex vivo (Extended Data Fig. 1a). Computationally determined clusters of cells (principal component analysis (PCA) followed by *t*-distributed stochastic neighbor embedding (*t*-SNE) visualization; Methods) were preferentially enriched for either unstimulated or stimulated cells; only cluster 5 contained nearly equal portions of both (Extended Data Fig. 1b). The degree of expansion observed among the clonotypes—that is,

the number of cells sharing the same clonotype in the dataset—associated strongly with phenotypic clusters of T cells determined on the basis of scRNA-seq (Fig. 3b). The most expanded clonotypes were observed in clusters 0 to 4. These clusters were enriched (compared to cluster 5) in genes associated with cytotoxic effector functions, such as *Gzmb* and *Id2*. The least-expanded clonotypes were concentrated in cluster 5, and were characterized by enrichments for genes encoding naïve or central memory markers, such as *Ccr7* and *Sell*[27] (compared to clusters 0–4) (Fig. 3b and Supplementary Fig. 3f). This association between the degree of clonal expansion and T cell activation affirms common principles of antigen-dependent activation among T cells[28].

Stimulated cells show clonotype-associated transcriptional profiles. To further investigate transcriptomic differences between the expanded clonotypes, we filtered the data to expanded clonotypes (detected in at least 15 cells) that were shared between the stimulated and the ex vivo groups (Fig. 3b–d). We also included 15 randomly sampled singletons (that is, clonotypes that were only detected once in the dataset) from the naïve cluster (cluster 5) in each stimulation condition, as a point of comparison. We examined the gene expression among these clonotypes ex vivo and after antigenic stimulation (Fig. 3d). We observed three groups of clonotypes associated with four modules of differentially expressed genes. Unsurprisingly, by comparing with annotated gene sets (MSigDB; Methods), we found that the sampled singletons (group 3) associated with a set of naïve and central memory T cell-related genes (for example, *Sell, Ccr7*; module 4) across both ex vivo and stimulated conditions[27]. We also observed another group (group 2) of clonotypes that strongly upregulated cell-cycle-related genes, characterized by *Myc* and *Myc*-targeted genes (module 1), after stimulation. The last group of clonotypes (group 1) exhibited higher expression of canonical cytotoxic effector markers, such as *Gzmb, Ccr2* and *Ccr5* (module 3), but only moderately upregulated genes in module 1 on stimulation[27] (Fig. 3d and Extended Data Fig. 1c). These observed signatures were also consistent with previously published signatures of effector CD8$^+$ T cells[29] (Supplementary Fig. 3g).

While module 2 and module 3 were both associated with phenotypes of effector T cells, module 2 contained markers of cytokine signaling and interferon response, such as *Irf7* and *Ifit1*, as opposed to the cytotoxic markers in module 3 (Fig. 3d). Module 2 was accordingly enriched in cytokine-mediated signaling signatures, while module 3 was enriched in cell motility signatures (Supplementary Fig. 3h). Module 3 was differentially expressed between group 1 and group 2 clonotypes, but module 2 was upregulated directly ex vivo for both groups of clonotypes. Downregulation of module 2 on stimulation may represent a transcriptional response to TCR-dependent activation[30]. We also note that group 1 clonotypes were also significantly more expanded than group 2 clonotypes, suggesting that the two groups of clonotypes may have experienced different levels of activation and expansion in vivo ($P < 0.001$ by Mann–Whitney *U*-test; Extended Data Fig. 2a). Overall, the clonotypes within groups 1 and 2 responded similarly on exposure to antigens; that is, similar genes were up- or downregulated on stimulation in both groups (Extended Data Fig 2b). The two groups of clonotypes differed, however, in the magnitude of transcriptional changes, particularly for genes in module 1 (*Myc*-related genes), and in the expression of genes in module 3 (cytotoxic-associated genes) (Fig. 3d and Extended Data Fig. 3c). Together, these results highlight how our method can further reveal clonotype-specific transcriptional responses not delineated by scRNA-seq alone.

Public clonotypes exhibit similar *CDR3* sequences. We next investigated public clones that were shared among the four animals. We detected 76 unique *Tcrb* sequences shared in at least two of the four animals (Extended Data Fig. 3a). We focused our analysis on the 21 clonotypes detected in at least three of the four mice (Supplementary Table 7). Amongst the public clones, we observed five sequences across the mice that exhibited clear convergence, wherein only two amino acid residues (the 7th and 8th residues) varied across the CDR3 sequences (Extended Data Fig. 3b). Amongst these, Leu-Gly accounts for 70% of cells, Ser/Ala/Gly-Gly for 20% and a shortened Asp-only sequence for the remaining 10%. Analysis of shared CDR3β sequences revealed variable pairing with CDR3α sequences both within and across mice, but several identical αβ pairings were observed in multiple animals (Extended Data Fig 3c). The most common CDR3β (CASSQDLGNYAEQFF) and its two distinct CDR3α partners (CAMREGLMATGGNNKLTF and CAVSNSGGSNYKLTF) were present in the same cells in three of the four animals ($n = 225$ cells; Extended Data Fig. 3c and Supplementary Table 8). These data suggest that these cells may possess dual-functional TCRα chains, a molecular feature that may play an important role in infection-induced autoimmunity[14,15,31].

Clonally expanded T cells detected in patients with peanut allergy. We next adapted the technique for use with human antigen-reactive CD4$^+$ T cells. Antigen-specific MHC tetramers are often not available for human T cells, making identification of disease-relevant T cells difficult compared to standard inbred mouse models. Instead, it is common to use either proliferation or expression of proteins associated with antigen-dependent activation (for example, CD154) as a proxy for the response to disease-relevant antigens[32,33]. We applied our approach to profile T cells isolated from patients with peanut allergy—a type 1 hypersensitivity condition linked to dysregulation of CD4$^+$ T cells[34]. Peripheral blood mononuclear cells (PBMCs) from four patients were incubated overnight with peanut antigens and then sorted for CD154$^+$ expression to enrich antigen-activated cells[32,33] (Supplementary Fig. 4a and Supplementary Table 9; Methods). Single-cell RNA-seq was then performed on the sorted cells via Seq-Well, and the corresponding *TCR* sequences were recovered (Supplementary Fig. 4b–d and Supplementary Table 10). We note that there were differences observed in the gene expression of cells from different patients, even after controlling for technical sources of variation (that is, sequencing depth, mitochondrial content; Methods). The differences observed were due in part to varied expression of a number of genes associated with basal cellular functions, including sex-linked genes (*XIST* and *RPS4Y1)* that were upregulated in cells from female and male subjects, respectively (Supplementary Fig. 4e and Supplementary Table 9). Overall, 2,712 cells from four patients were included in the analysis. Contrary to what was observed for the tetramer-sorted mouse cells, the majority of the human CD154$^+$ T cells were not clonal (mean = 75 ± 12%). One of the patients (patient 77) exhibited a substantial expansion of T cells sharing common *TCR* sequences relative to the others (all patients: Supplementary Fig. 4b,c; patient 77: Fig. 4a). These clonally expanded T cells expressed genes associated with activation, such as *CD154*, *CD69* and *TNFRSF4*, as well as *GATA3*, a transcription factor associated with T_H2 cells[32,35]. In contrast, the nonexpanded cells exhibited genes associated with central memory or naïve cells, including *CCR7*, *SELL* and *LEF1* (refs. [36,37]) (Fig. 4b). Composite scores of known signatures of CD4$^+$ T cell subtypes confirmed an enrichment of T_H2 signature in some of the expanded T cells[38] (Supplementary Fig. 4f).

Expanded clonotypes exhibit varied expression of T_H2 genes. To examine whether these heterogeneous T cells from patient 77 might represent a spectrum of activation states, we next performed pseudotemporal analysis that showed a trajectory correlated with the degree of T cell stimulation, marked by increased expression of *JUN*, *FOS*, *NFKB* and *CD154*, among others[32,39] (Extended Data Fig. 4). Genes associated with early pseudotime were enriched in canonical markers for naïve T cells, while genes associated with late pseudotime

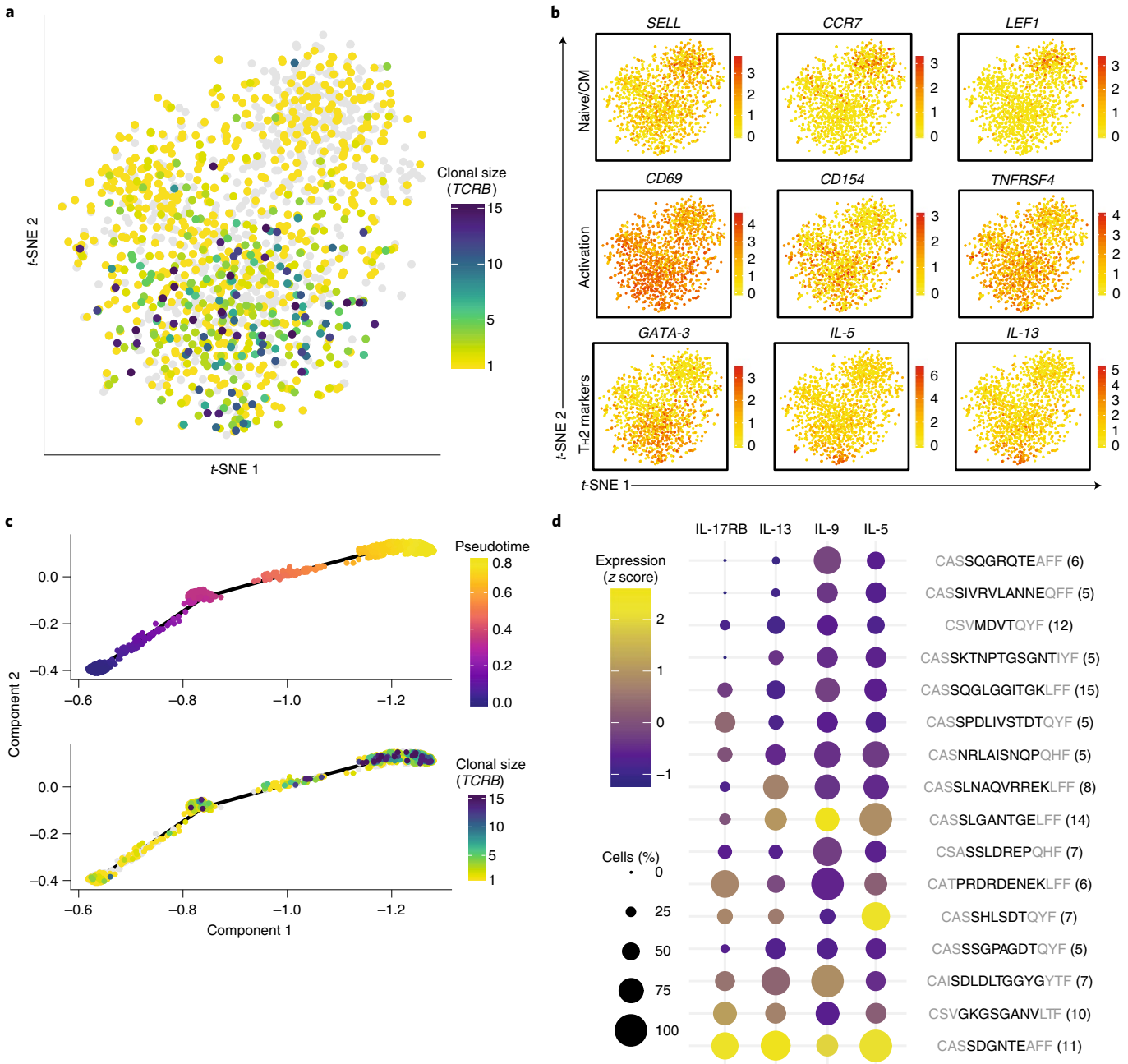

Fig. 4 | ScRNA-seq and TCR analysis of peanut-dependent activated T cells from one of the individuals with an allergy to peanut (patient 77) combined with pseudotemporal analysis. a, Clonal size of *TCRB* clonotypes mapped onto *t*-SNE visualization of transcriptomic data ($n = 1{,}496$ cells). **b**, Expression of canonical markers associated with naïve/central memory, T cell activation and T_H2 phenotypes. Color indicates log-normalized gene expression (yellow to red). **c**, Pseudotime trajectory (top) of scRNA-seq results with *TCRB* clonal size mapped (bottom). **d**, T_H2 pathogenic marker expression amongst expanded ($n \geq 5$ cells per clonotype, resulting in 16 total clonotypes included) *TCRB* clonotypes with high pseudotime value (mean > 0.4, see Extended Data Fig. 5b). Gene expression represents averages within each clonotype group and scaled across all groups. Structural amino acids shown in gray. Number of cells shown in parentheses. Color indicates scaled and log-normalized gene expression (purple to yellow).

were enriched in markers for effector T cells (Extended Data Fig. 5a). The T cells most associated with activation on the trajectory were also the most clonally expanded ($r_s = 0.39$, $n = 851$, $P < 0.001$ by Spearman; Fig. 4c). Further, our pseudotemporal trajectory correlated strongly with expression of *IL-5*, *IL-9*, *IL-13* and *IL-17RB*, known to encode markers of pathogenic T_H2 cells[34,35] (Extended Data Fig. 4, cluster 1). From these data, we posit that clonotypes that are both expanded and located towards the end of the trajectory may enumerate activated peanut-specific T cells. Among such cells, a subset of clonotypes exhibited T_H2 functional signatures (Fig. 4d). In particular, only one clonotype (CASSDGNTEAFF) had high expression for all four T_H2 markers, suggesting a robust polyfunctionality that may represent a highly differentiated T_H2-polarized clone involved in the allergic state of the individual[40,41]. Although the majority of expanded clonotypes were located at the end of the pseudotime trajectory, we noted that some clonotypes showed higher variation in phenotypic states than others (Extended Data Fig. 5b). It is possible that other factors may also contribute to the observed cell state and expansion of these T cells, such as transcriptional pulsing or bystander activation[42–44]. Taken together, our data

suggest that our method can resolve differential degrees of antigen-dependent activation among clonotypes from human T cells and potentially highlight clonotypes among enriched pools of activated T cells that are most relevant to a disease state of interest.

Discussion

Our approach allows for the reliable recovery of *TCR CDR3* sequences from 3′-barcoded scRNA-seq samples generated by Seq-Well or related common, massively parallel 3′ scRNA-seq methods, such as Drop-seq. With minor modifications, our method should adapt to other 3′-based sequencing methods. We recapitulated pairings of known *Tcra* and *Tcrb* chains in transgenic murine models, and found transcriptomic signatures that were associated with clonally expanded T cells bearing the same TCRs in both murine and human samples. We note that there was a distinct difference in the magnitude of clonal expansion observed between the murine and human samples. This observed variation likely reflects both the difference in methods used for enrichment of antigen-reactive T cells (MHC tetramer staining versus CD154 enrichment) and in the history of antigen exposure in vivo (immunization versus peanut avoidance).

Our method relies on simple and inexpensive reagents that are widely available and can be used to sequence the variable regions of TCRs for both new and preexisting whole-transcriptome-amplified products. As such, our method is also compatible with other multiplex, high-throughput scRNA-seq techniques, such as antibody-based cell hashing[45]. Future experiments combining the approach we present here with other technologies, such as germline genomic barcoding, should allow further mechanistic studies of TCR clonotypic responses. Such strategies could further illuminate the degree to which TCR sequence (that is, shared antigen recognition) versus clonotypic identity (that is, cell lineage) shapes the trajectories of phenotypes accessible in health and disease[46].

In addition to its simplicity, our approach also targets sequencing reads to the *CDR3* region of the transcripts, allowing for deep sequencing of clonotypes with high efficiency using ubiquitous, high-accuracy, short-read sequencing technologies. Because our method does not rely on amplification with multiplexed primer pools (used for a single extension to append UPS2), it minimizes amplification bias and artifacts introduced by these primers, maximizing the complexity and efficiency of the sequencing pools[4,47]. Similarly, since it relies on a universal primer element for PCR amplification (UPS2 and a modified UPS), the method simplifies adaptation to other model species, such as nonhuman primates, by minimizing the need for additional optimization with new multiplex pools of primers. Finally, we foresee that our general approach can also be used for other targets where isoform information is paramount, such as identification of *CD45RA* or *CD45RO* in T cells[48].

Nonetheless, there are currently two practical limitations. First, the innate efficiency of capturing mRNA using available reagents (that is, 3′-barcoded beads for Seq-Well and Drop-seq) limits the maximum potential representation (and thus recovery) of TCRs in libraries. Currently, for Drop-seq, it is estimated that the barcoded beads capture 10–12% of available transcripts[16]. Improved quality of these reagents or of the molecular biology used to generate WTA products will likely address this limitation[24]. Second, due to the incorporation of V-region primers, the method presently does not recover full-length *TCR* transcripts, and therefore our analysis is restricted to the *CDR3* region. The *CDR3* region contains the majority of variability in *TCR* transcripts, and, therefore, is likely sufficient for assessing clonal expansion and clonal tracking analysis[47]. Further, the design of the V-region primers depends on adequate annotation of V genes, which may not be available for less well-characterized model species. Although we expect characterization of V genes in many species to improve in the future, approaches using 5′ scRNA-seq can employ constant-region primers, thus circumventing the need for V-region primers altogether. For these 5′ cellular-barcoding approaches, our methodology, modified to use baits targeting TCR constant regions, could potentially aid in more efficient TCR characterization.

In summary, we have developed a simple approach to recover *TCR CDR3* sequences from whole-transcriptome libraries produced by common high-throughput scRNA-seq techniques that rely on 3′ barcoding of transcripts. We found the technique to be reliable and also high yielding, limited predominantly by the efficiency of the initial capture of mRNA. Our approach can map murine and human antigen-reactive T cells, and, in principle, is extensible to other species (for example, nonhuman primates) and target genes of interest (for example, viral antigens, isoforms, germline and somatic variations of B cell receptors). Extension of this technique should be feasible, as long as the targeted variable regions are flanked by suitable known sequences. Overall, our data demonstrate that enhancing the resolution of these populations of cells by the combined recovery of *TCRs* and scRNA-seq can further reveal phenotypic variations that emerge as a function of clonotype, and reveal convergent public clones with precision. We anticipate that our method will be especially useful for elucidating the intrinsic heterogeneity among antigen-specific T cells and their roles in immunological diseases, such as cancer, autoimmune disorders and food allergy.

Online content

Any methods, additional references, Nature Research reporting summaries, source data, extended data, supplementary information, acknowledgements, peer review information; details of author contributions and competing interests; and statements of data and code availability are available at https://doi.org/10.1038/s41590-019-0544-5.

Received: 26 March 2019; Accepted: 21 October 2019;
Published online: 19 November 2019

References

1. Schrama, D., Ritter, C. & Becker, J. C. T cell receptor repertoire usage in cancer as a surrogate marker for immune responses. *Semin. Immunopathol.* **39**, 255–268 (2017).
2. Lossius, A. et al. High-throughput sequencing of TCR repertoires in multiple sclerosis reveals intrathecal enrichment of EBV-reactive CD8$^+$ T cells. *Eur. J. Immunol.* **44**, 1–41 (2014).
3. Kirsch, I. R. et al. TCR sequencing facilitates diagnosis and identifies mature T cells as the cell of origin in CTCL. *Sci. Transl. Med.* **7**, 1–13 (2015).
4. Carlson, C. S. et al. Using synthetic templates to design an unbiased multiplex PCR assay. *Nat. Commun.* **4**, 2680 (2013).
5. Crosby, E. J. et al. Complimentary mechanisms of dual checkpoint blockade expand unique T-cell repertoires and activate adaptive anti-tumor immunity in triple-negative breast tumors. *Oncoimmunology* **7**, e1421891 (2018).
6. Tirosh, I. et al. Dissecting the multicellular ecosystem of metastatic melanoma by single-cell RNA-seq. *Science* **352**, 189–196 (2016).
7. Khodadoust, M. S. et al. Antigen presentation profiling reveals recognition of lymphoma immunoglobulin neoantigens. *Nature* **543**, 723–727 (2017).
8. Avraham, R. et al. Pathogen cell-to-cell variability drives heterogeneity in host immune responses. *Cell* **162**, 1309–1321 (2015).
9. Papalexi, E. & Satija, R. Single-cell RNA sequencing to explore immune cell heterogeneity. *Nat. Rev. Immunol.* **18**, 35–45 (2017).
10. Shalek, A. K. et al. Single-cell transcriptomics reveals bimodality in expression and splicing in immune cells. *Nature* **498**, 236–240 (2013).
11. Azizi, E. et al. Single-cell map of diverse immune phenotypes in the breast tumor microenvironment. *Cell* **174**, 1293–1308.e36 (2018).
12. Zhang, L. et al. Lineage tracking reveals dynamic relationships of T cells in colorectal cancer. *Nature* **564**, 268–272 (2018).
13. Han, A., Glanville, J., Hansmann, L. & Davis, M. M. Linking T-cell receptor sequence to functional phenotype at the single-cell level. *Nat. Biotechnol.* **32**, 684–692 (2014).
14. Stubbington, M. J. T. et al. T cell fate and clonality inference from single-cell transcriptomes. *Nat. Methods* **13**, 329–332 (2016).
15. Dash, P. et al. Paired analysis of TCRα and TCRβ chains at the single-cell level in mice. *J. Clin. Invest.* **121**, 288–295 (2011).
16. Macosko, E. Z. et al. Highly parallel genome-wide expression profiling of individual cells using nanoliter droplets. *Cell* **161**, 1202–1214 (2015).

17. Klein, A. M. et al. Droplet barcoding for single-cell transcriptomics applied to embryonic stem cells. *Cell* **161**, 1187–1201 (2015).
18. Gierahn, T. M. et al. Seq-well: portable, low-cost RNA sequencing of single cells at high throughput. *Nat. Methods* **14**, 395–398 (2017).
19. Saikia, M. et al. Simultaneous multiplexed amplicon sequencing and transcriptome profiling in single cells. *Nat. Methods* **16**, 59–62 (2019).
20. Singh, M. et al. High-throughput targeted long-read single cell sequencing reveals the clonal and transcriptional landscape of lymphocytes. *Nat. Commun.* **10**, 3120 (2019).
21. Zemmour, D. et al. Single-cell gene expression reveals a landscape of regulatory T cell phenotypes shaped by the TCR. *Nat. Immunol.* **19**, 291–301 (2018).
22. Jain, M. et al. Nanopore sequencing and assembly of a human genome with ultra-long reads. *Nat. Biotechnol.* **36**, 338–345 (2018).
23. Gupta, I. et al. Single-cell isoform RNA sequencing characterizes isoforms in thousands of cerebellar cells. *Nat. Biotechnol.* **36**, 1197–1202 (2018).
24. Hughes, T. K. et al. Highly efficient, massively-parallel single-cell RNA-seq reveals cellular states and molecular features of human skin pathology. Preprint at *bioRxiv* https://doi.org/10.1101/689273 (2019).
25. Blüthmann, H. et al. T-cell-specific deletion of T-cell receptor transgenes allows functional rearrangement of endogenous α- and β-genes. *Nature* **334**, 156–159 (1988).
26. Dash, P. et al. Quantifiable predictive features define epitope-specific T cell receptor repertoires. *Nature* **547**, 89–93 (2017).
27. Mousset, C. M. et al. Comprehensive phenotyping of T cells using flow cytometry. *Cytometry A* **95**, 647–654 (2019).
28. Farber, D. L., Yudanin, N. A. & Restifo, N. P. Human memory T cells: generation, compartmentalization and homeostasis. *Nat. Rev. Immunol.* **14**, 24–35 (2014).
29. Singer, M. et al. A distinct gene module for dysfunction uncoupled from activation in tumor-infiltrating T cells. *Cell* **166**, 1500–1511.e9 (2016).
30. Huang, W. & August, A. The signaling symphony: T cell receptor tunes cytokine-mediated T cell differentiation. *J. Leukoc. Biol.* **97**, 477–485 (2015).
31. Padovan, E. et al. Expression of two T cell receptor alpha chains: dual receptor T cells. *Science* **262**, 422–424 (1993).
32. Bacher, P. & Scheffold, A. Flow-cytometric analysis of rare antigen-specific T cells. *Cytometry A* **83A**, 692–701 (2013).
33. Chattopadhyay, P. K., Yu, J. & Roederer, M. Live-cell assay to detect antigen-specific CD4$^+$ T-cell responses by CD154 expression. *Nat. Protoc.* **1**, 1–6 (2006).
34. Syed, A., Kohli, A. & Nadeau, K. C. Food allergy diagnosis and therapy: where are we now? *Immunotherapy* **5**, 931–944 (2013).
35. Seumois, G. et al. Transcriptional profiling of Th2 cells identifies pathogenic features associated with asthma. *J. Immunol.* **197**, 655–664 (2016).
36. Mueller, S. N., Gebhardt, T., Carbone, F. R. & Heath, W. R. Memory T cell subsets, migration patterns, and tissue residence. *Annu. Rev. Immunol.* **31**, 137–161 (2013).
37. Nish, S. A. et al. CD4$^+$ T cell effector commitment coupled to self-renewal by asymmetric cell divisions. *J. Exp. Med.* **214**, 39–47 (2017).
38. Wei, G. et al. Global mapping of H3K4me3 and H3K27me3 reveals specificity and plasticity in lineage fate determination of differentiating CD4$^+$ T cells. *Immunity* **30**, 155–167 (2009).
39. Foletta, V. C., Segal, D. H. & Cohen, D. R. Transcriptional regulation in the immune system: all roads lead to AP-1. *J. Leukoc. Biol.* **63**, 139–152 (1998).
40. Müller, U. et al. Lack of IL-4 receptor expression on T helper cells reduces T helper 2 cell polyfunctionality and confers resistance in allergic bronchopulmonary mycosis. *Mucosal Immunol.* **5**, 299–310 (2012).
41. Upadhyaya, B., Yin, Y., Hill, B. J., Douek, D. C. & Prussin, C. Hierarchical IL-5 expression defines a subpopulation of highly differentiated human Th2 cells. *J. Immunol.* **187**, 3111–3120 (2011).
42. Ritvo, P.-G. et al. High-resolution repertoire analysis reveals a major bystander activation of Tfh and Tfr cells. *Proc. Natl Acad. Sci. USA* **115**, 9604–9609 (2018).
43. Raj, A. & van Oudenaarden, A. Nature, nurture, or chance: stochastic gene expression and its consequences. *Cell* **135**, 216–226 (2008).
44. Han, Q. et al. Polyfunctional responses by human T cells result from sequential release of cytokines. *Proc. Natl Acad. Sci. USA* **109**, 1607–1612 (2012).
45. Stoeckius, M. et al. Cell hashing with barcoded antibodies enables multiplexing and doublet detection for single cell genomics. *Genome Biol.* **19**, 224 (2018).
46. Schumacher, T. N. M., Gerlach, C. & van Heijst, J. W. J. Mapping the life histories of T cells. *Nat. Rev. Immunol.* **10**, 621–631 (2010).
47. Rosati, E. et al. Overview of methodologies for T-cell receptor repertoire analysis. *BMC Biotechnol.* **17**, 61 (2017).
48. Hermiston, M. L., Xu, Z. & Weiss, A. CD45: a critical regulator of signaling thresholds in immune cells. *Annu. Rev. Immunol.* **21**, 107–137 (2003).

Publisher's note Springer Nature remains neutral with regard to jurisdictional claims in published maps and institutional affiliations.

© The Author(s), under exclusive licence to Springer Nature America, Inc. 2019

Methods

Mouse splenocyte processing for OT-I spiked-in experiments. Spleens were taken from C57BL/6NTac (Taconic) wild-type (WT) mice and B6 *Rag1*$^{+/+}$*Rag2*$^{+/+}$ OT-I (C57BL/6-Tg; Jackson) transgenic mice. Mice were male and at age 8–12 weeks. T cells from each spleen were isolated using magnetic bead-based enrichment (StemCell; catalog no. 19853). Cell concentration was estimated by counting on a hemocytometer. Four mixes of WT and OT-I cells were made with 10%, 1%, 0.1% and 0.01% of OT-I T cells. Each cell mixture was processed via Seq-Well as previously described[18]. No OT-I *Tcra* or *Tcrb* chain was observed in the 0.01% spiked-in sample. The resulting single-cell libraries were sequenced on the Illumina NextSeq 500, as previously described. Part of the constructed libraries was used for *TCR* recovery as described below. All animal work was conducted under the approval of the Massachusetts Institute of Technology Division of Comparative Medicine in accordance with federal, state and local guidelines (CAC protocols no. 01717-076-20, no. 0917-092-20).

Mouse splenocyte processing for HPV-E7 experiment. C57BL/6NTac (Taconic) mice (female, 8 weeks of age) were primed with 100 µg of MSA-E7 and 25 µg of cyclic di-GMP subcutaneously in the tail base (day 0). The mice were boosted with the same mixture at day 14, and at day 20 spleens from the mice were collected. Splenocytes were stimulated for 6 h with 10 µg ml^{-1} of E7 peptide (RAHYNIVTF) in RPMI with 10% FBS. The cells were then stained with anti-CD8-APC (clone 53–6.7; BioLegend) and E7-tetramer-PE (MBL; catalog no. TB-5008-2) and flow sorted with a FACSAria II instrument (BD Biosciences) for double-positive T cells. The sorted cells were processed via an updated version of Seq-Well (Seq-Well S^3)[24]. All animal work was conducted under the approval of the MIT Division of Comparative Medicine in accordance with federal, state and local guidelines (CAC protocols no. 01717-076-20, no. 0917-092-20).

Human subjects. The human subjects in this study were all screened for participation in a peanut oral immunotherapy trial (NCT01750879), and some were included in a high-threshold peanut challenge study (NCT02698033), at the Food Allergy Center at Massachusetts General Hospital. All subjects were recruited with informed consent, and the study was approved by the Institutional Review Board of Partners Healthcare (protocol no. 2012P002153) and MIT (protocol no. 1312006071). The participants all had a previous diagnosis of peanut allergy, a history of peanut-induced reactions consistent with immediate hypersensitivity and confirmatory peanut- and Ara h 2 (a dominant peanut allergen)-specific serum IgE concentrations (>0.35 kU$_A$ l^{-1}; ImmunoCAP; Thermo Fisher). Blood samples were taken at the time of patient intake, before any treatment of peanut allergy.

Human PBMC processing for allergy samples. PBMCs were isolated from patient blood samples by density gradient centrifugation (Ficoll-Paque Plus; GE Healthcare). Fresh PBMC were cultured in AIM V medium (Gibco) for 20 h with 100 µg ml^{-1} peanut protein extract. The peanut extract was prepared by agitating defatted peanut flour (Golden Peanut and Tree Nuts) with PBS, centrifugation and sterile filtering. Anti-CD154-PE (clone TRAP1; BD Biosciences) was added to the cultures for the last 3 h. After collecting, the cells were labeled with anti-CD3-AF700 (clone UCHT1), anti-CD4-APC-Cy7 (RPA-T4), anti-CD45RA-FITC (HI100), anti-CD154-PE (all from BD Biosciences), anti-CD69-AF647 (FN50; BioLegend) and Live/Dead Fixable Violet stain (L34955; Thermo Fisher). Live CD3$^+$CD4$^+$CD45RA$^-$-activated CD154$^+$ cells were sorted with a FACSAria II instrument (BD Biosciences). The sorted cells were processed via Seq-Well[18].

Enrichment of *TCR* transcripts. Enrichment of TCR-encoding transcripts from whole-transcriptome amplified starting materials was done with xGen Lockdown reagents (IDT; catalog no. 1072281), with modifications. Biotinylated *TCRA-TCRB* probes were purchased (IDT Ultramer Services; Supplementary Table 1), mixed and diluted to 1.5 µM each. Up to 3.5 µl of WTA was added to 8.5 µl of xGen 2× hybridization buffer, 2.7 µl of buffer enhancer, 0.8 µl of UPS primer (50 µM; Supplementary Table 2) and 0.5 µl of human cot-1 DNA (Invitrogen; catalog no. 15279011). The mixture was incubated at 95 °C for 10 min, and 1 µl of diluted TCRC mix was added. The final mixture was then incubated at 65 °C for 1 h. Then, the remainder of the xGen Lockdown protocol was followed. A 50 µl portion of streptavidin Dynabeads (Invitrogen; catalog no. 65306) was used for each sample. Each sample was eluted into 20 µl of water.

To amplify the *TCRA* and *TCRB* transcripts after enrichment, five PCR reactions were done for each enriched sample with the following composition: 2 µl of eluted sample, 2 µl of UPS primer (10 µM), 8.5 µl of water and 12.5 µl of 2× Kapa Hifi Hotstart Readymix (Kapa Biosystems). The following PCR cycling conditions were used: 1 cycle of 95 °C for 3 min; 25 cycles of 98 °C for 40 s, 67 °C for 20 s, 72 °C for 1 min; 1 cycle of 72 °C for 5 min. The five reactions were then pooled to a final volume of 100 µl. Products of >1,000 base pairs (bp) were purified using homemade purification reagents outlined by Rohland and Reich[49]. The purified product was eluted into 15 µl of water. The quality of the final product was assessed using a fragment analyzer (Advanced Analytical/Agilent).

Construction of *TCR* sequencing libraries. TCRV-UPS2 primers were purchased[13,15] (Eurofin; Supplementary Table 3). Two primer mixes were made (one for *TCRB* and one for *TCRA*) and diluted to 10 µM each. *TCRA* and *TCRB* reaction mixes were made with 4 µl of purified enriched product, 6 µl of water, 2.5 µl of TCRV-UPS2 primer mix (*TCRA* or *TCRB*) and 12.5 µl of 2× Kapa Readymix. Primer extension was done with the following conditions: 1 cycle of 98 °C for 5 min, 1 cycle of 55 °C for 30 s and 1 cycle of 72 °C for 2 min. The final product was purified as previously described, and eluted into 11 µl of water.

Complete sequencing handles were added to the final product using the following PCR mix: 0.5 µl of UPS2-N70x primer (10 µM), 0.5 µl of UPS2-N50x primer (10 µM), 9 µl of water and 12.5 µl of 2× Kapa readymix were added to 2.5 µl of previously eluted products. Four reactions were performed for each sample, using a total of 10 µl of eluted products. Amplification was done using the following cycling conditions: 1 cycle of 95 °C for 2 min; 12–15 cycles of 95 °C for 30 s, 60 °C for 30 s and 72 °C for 1.5 min; and 1 cycle of 72 °C for 5 min. All four reactions were pooled and purified for products >1,000 bp, as previously described. Final product was assessed using a fragment analyzer, and a major peak of around 1,100 bp was observed for the *TCRB* product and of 1,300 bp for the *TCRA* products. Library concentrations were assessed using the Kapa Library qPCR quantification kit (Kapa Biosystems). A more detailed step-by-step protocol (including example size distributions of successfully amplified samples) is available at http://shaleklab.com/resources/ and on the Nature Protocol Exchange.

Conditions for TCR sequencing. *TCRA* and *TCRB* libraries were pooled at equimolar concentration. For single-end sequencing, 1–2 nmol of the final library was used to sequence on the Illumina MiSeq. A total of 150 cycles was performed on read 1 using the TCR-specific sequencing primers, and 20 cycles were performed on index 1 using Seq-Well sequencing primer (Supplementary Table 4). Sequencing primers were used at a final concentration of 2.5 µM. We aimed for 8–12 × 10^6 pass filter reads per lane (cluster density of roughly 450 K mm^{-2}). On the basis of the whole-transcriptome data, we allotted ~6,000 T cells per lane.

Assessment of TCR transcript enrichment. A qPCR assay was used to assess enrichment of *TCRA* or *TCRB* transcripts after affinity enrichment. Three rounds of TCR affinity enrichment were performed as described. TaqMan Fast Advanced Master Mix (Applied Biosystems; catalog no. 4444556) was used along with FAM TaqMan primer mixes (*TCRA*, HS00354482_m1; *TCRB*, HS01588269_g1; *GAPDH*, HS02758991_g1). Amplification was done according to the manufacturer's instruction. qPCR was done before and after TCR enrichment, and the difference in crossing point (ΔCp) for *TCR* and *GAPDH* was calculated. ΔCp for each of the enriched samples was compared to that of the unenriched sample, and the difference was calculated (ΔΔCp). ΔΔCp was used to calculate relative increase in concentration of *TCR* transcripts after enrichment, compared to *GAPDH*.

Determination of clonotypes from sequencing data. *TCR* sequencing data were filtered by mapping to the TCR-encoding loci (chromosome *TCRB* 7 and *TCRA* 14 for human, and *Tcrb* 6 and *Tcra* 14 for mouse, respectively). The filtered data were categorized by cell barcodes and UMIs. Cell barcodes and UMIs with at least ten filtered reads were kept and the rest were discarded. Each set of reads was then mapped to *TCRV* and *TCRJ* IMGT (imgt.org) reference sequences via IgBlast, and mapping to each V and J region was tabulated. The reads were then filtered for 'strong plurality', wherein the ratio of the most frequent V and J calls to the second most frequent calls was calculated, resulting in a possible value of 0.5 to 1. Cell barcodes with top V and J calls with a ratio of greater than 0.6 were kept, and the rest were filtered out. Within each cell barcode group, reads with the top V and J calls were then used for CDR3 calling, and a similar ratio was calculated on the basis of the nucleotide sequence (Supplementary Fig. 2c). For CDR3 calling, nucleotides corresponding to the cysteine at position 104 and phenylalanine at position 118 were identified according to IMGT references, and amino acid sequences in between the residues were translated. *TCR* sequences were then matched to single-cell data via the cell barcodes. If multiple *TCR* α and β chains were detected for a cell barcode, the *TCRβ* sequences with the highest number of UMIs and raw reads mapping were kept. Up to two *TCRα* sequences with the top two highest numbers of UMIs and raw reads mapping were kept. We note that nonfunctional CDR3 regions (that is, CDR3 sequences with stop codon or out-of-frame sequences) are often a result of initially unsuccessful V(D)J recombination, and are often shared in clonal cells[15]. As such, nonfunctional CDR3 regions were excluded from additional functional phenotype analysis, but used as unique markers for clonal tracking. Read depth and number of UMIs recovered for each of the CDR3 regions for each of the mouse and human samples are shown in Supplementary Fig. 5b,d.

Data analysis for transcriptomic data. Single-cell transcriptomic data were processed using Drop-seq tools (http://mccarrolllab.com/dropseq) as previously described[16,18]. In brief, barcodes and UMIs were collapsed with a single-base error tolerance. Cells with less than 500 detected genes and 1,000 UMIs were filtered. The resulting data were then natural log-normalized for each cell to account for library size, and variances due to detected mitochondrial genes were regressed from the data.

Single-cell analysis of T cells from mice immunized with HPV-E7. Single-cell analysis was performed as previously described, with modifications[18]. The

modifications were as follows: we identified 461 variable genes with log-mean expression values greater than 0.1 and dispersion (variance/mean) of greater than 1. PCA was performed on the variable genes using the RunPCA function in Seurat. Principal components (PCs) were analyzed with the PCElbowPlot function in Seurat, and five significant components were identified. A two-dimensional *t*-SNE visualization was then generated from the PC loadings for these first five PCs. Clusters were identified using the FindClusters function in Seurat with a resolution of 0.4. Genes shown in Fig. 3d were chosen by using the FindAllMarkers function in Seurat using the previously defined clusters. The resulting list was filtered for genes that show an average fold change greater than 2 with an adjusted *P* value of less than 0.001. To calculate gene expression by clonotypes, normalized gene counts of cells sharing the same clonotypes were averaged. Then, each gene was scaled to produce a *z* score with maximum and minimum of +2 and −2, respectively. The clonotype gene expression was clustered using ward.D2. Modules 2 and 3 were also separately queried against the C5 reference set. Signatures from Singer et al.[29] were implemented on the dataset using the AddModuleScore function in Seurat (Supplementary Table 11). Numbers of genes, UMIs, reads and percentage of mitochondrial genes recovered for each sample are shown in Supplementary Fig. 5a.

Single-cell analysis of T cells in peanut allergy. Single-cell analysis was performed as previously described, with modifications[18]. The modifications were as follows: for datasets including all four patients, we identified 486 genes with log-mean expression values greater than 0.1 and dispersion (variance/mean) of greater than 1. PCA was performed on the variable genes using the RunPCA function in Seurat. A two-dimensional *t*-SNE visualization was then generated from the PC loadings of the 20 most significant PCs. For patient 77, we identified 701 variable genes with log-mean expression values greater than 0.1 and dispersion (variance/mean) of greater than 1. PCA was performed on the variable genes using the RunPCA function in Seurat. PCs were analyzed with the PCElbowPlot function in Seurat, and 15 significant components were identified. A two-dimensional *t*-SNE visualization was then generated from the PC loadings for these first 15 PCs. UMAP was also separately applied to the loadings of these identified principal components. The cluster of T cells with the highest clonal expansion was used for pseudotemporal analysis using Monocle 3 (ref. [50]). UMAP dimension reduction was used for pseudotemporal analysis, as suggested by the authors of Monocle 3. Trajectory was calculated using the implementation of DDRTree in the learnGraph function in Monocle. Signatures from Wei et al. [38] were implemented using the AddModuleScore function in Seurat (Supplementary Table 11). Numbers of genes, UMIs, reads and percentage of mitochondrial genes recovered for each sample are shown in Supplementary Fig. 5c.

MSigDB signature enrichment analysis. Genes of interest (modules from Fig. 3, clusters 3 and 4 from Extended Data Fig. 4) were queried against gene sets from MSigDB to calculate significant overlap of gene signatures[51,52]. For the murine dataset, modules 2, 3 and 4 were compared against H, C2 and C7 reference sets. The results were filtered for signatures relevant to T cells, and the top five most significant signatures for each module are shown in Extended Data Fig. 1c. Module 1 was compared against the H reference set, and the top five most significant signatures are shown in Extended Data Fig. 1c. For the human dataset, clusters 3 and 4 were compared against the C7 reference set. The results were filtered for signatures relevant to T cells, and the top ten most significant signatures for each cluster are shown in Extended Data Fig. 5a. Each signature was manually assigned a short description to aid visualization. Full MSigDB overlap calculation results, as well as the manually assigned description, are available in Supplementary Table 12.

Statistics and reproducibility. R was used for statistical analysis. Specific statistical tests are indicated in the figure legends and corresponding sections in the main text. Circlize was used for TCR circus plots[53]. All confidence intervals were calculated by standard deviation unless otherwise indicated. All box and whisker plots indicate the (box) 25th and 75th percentile along with (whisker) ±1.5× interquartile range, unless otherwise indicated. For OT-I T cell analysis in Fig. 2a, the recovery percentage was calculated by dividing the number of cells with OT-I *Tcra* or *Tcrb CDR3* by the total number of cells with recovered *Tcra* or *Tcrb CDR3* sequences. One cell with OT-I *CDR3β* was detected in the 0.01% spiked-in sample. For the OT-I T cell analysis in Fig. 2b, two doublet cells were excluded from the analysis. For the OT-I T cell analysis in Supplementary Fig. 2a, the predicted rate of recovery for both TCRα and TCRβ chains was calculated by multiplying the rates of individual recovery and summing the variance of each chain. Clustering of the heat map in Fig. 3d was done on the data of stimulated cells, and superimposed on the ex vivo portion. Clonotypes in group 1 were randomly downsampled to 15 clones to aid visualization. Spearman's correlation between *TCRB* clonal size and pseudotime in human peanut allergy samples was calculated using T cells with recovered *TCRB*. All adjusted *P* values were calculated using the Bonferroni correction, unless noted otherwise.

Reporting Summary. Further information on research design is available in the Nature Research Reporting Summary linked to this article.

Data availability

FASTQ file format data related to murine samples are available through GEO and BioProject under accession numbers GSE136028 and PRJNA560970. FASTQ file format data related to human samples is available through dbGaP under accession number phs001897.v1.p1. Source data files and associated metadata tables for Figs. 2–4 are available on http://shaleklab.com/resources/, https://github.com/mitlovelab/ or upon request. MSigDB results for Extended Data Fig. 1c, Extended Data Fig. 5a and Supplementary Fig. 3h are available as Supplementary Table 12. Full results from the differential gene expression comparison shown in Extended Data Fig. 2c are available as Supplementary Table 13. All recovered CDR3 sequences, and their frequencies, of *TCR* α and β chains from E7-immunized mice and patients with peanut allergy are available as Supplementary Tables 6 and 10. Gene expression matrices for E7-immunized mice and patients with peanut allergy are available as Supplementary Data 1 and 2.

Code availability

R scripts for generating all analysis, Matlab scripts for processing TCR sequencing data, as well as all updates, are available at http://shaleklab.com/resources/, https://github.com/mitlovelab/ or upon reasonable request.

References

49. Rohland, N. & Reich, D. Cost-effective, high-throughput DNA sequencing libraries for multiplexed target capture. *Genome Res.* **22**, 939–946 (2012).
50. Qiu, X. et al. Reversed graph embedding resolves complex single-cell trajectories. *Nat. Methods* **14**, 979–982 (2017).
51. Liberzon, A. et al. Molecular signatures database (MSigDB) 3.0. *Bioinformatics* **27**, 1739–1740 (2011).
52. Liberzon, A. et al. The Molecular Signatures Database hallmark gene set collection. *Cell Syst.* **1**, 417–425 (2015).
53. Gu, Z., Gu, L., Eils, R., Schlesner, M. & Brors, B. circlize implements and enhances circular visualization in R. *Bioinformatics* **30**, 2811–2812 (2014).

Acknowledgements

We thank P. Blainey and M. Birnbaum for fruitful discussions. This work was supported in part by the Koch Institute Support (core) NIH Grant P30-CA14051 from the National Cancer Institute, as well as the Koch Institute - Dana-Farber/Harvard Cancer Center Bridge Project. This work was also supported by the Food Allergy Science Initiative at the Broad Institute and the NIH (5P01AI039671, 5U19AI089992, U19AI095261). A.K.S. was supported by the Searle Scholars Program, the Beckman Young Investigator Program, the Pew-Stewart Scholars Program for Cancer Research, a Sloan Fellowship in Chemistry, the NIH (1DP2GM119419, 2U19AI089992, 2R01HL095791, 1U54CA217377, 2P01AI039671, 5U24AI118672, 2RM1HG006193, 1R33CA202820, 1R01AI138546, 1R01HL134539, 1R01DA046277, 1U2CCA23319501) and Agilent Technologies.

Author contributions

A.A.T., T.M.G, A.K.S. and J.C.L. developed the concepts and designed the study. A.A.T. and T.M.G. performed the experiments. A.A.T. prepared the manuscript with input from all authors. A.A.T., T.M.G., B.M. and D.M.M. performed bioinformatics analyses. N.K.M. performed E7 immunization of mice. W.G.S. designed the clinical study and provided samples from peanut-allergic patients. B.R. performed stimulation and sorting of PBMCs from allergic patients.

Competing interests

A.A.T., T.M.G., J.C.L. and the Massachusetts Institute of Technology have filed a patent application (patent no. PCT/US2018/013443) that relates to T cell receptor recovery, compositions of matter and the outlined experimental and computational methods and uses thereof. J.C.L. and A.K.S. are co-founders and shareholders of Honeycomb Biotechnologies, Inc. T.M.G. is currently an employee of Honeycomb Biotechnologies, Inc.

Additional information

Extended data is available for this paper at https://doi.org/10.1038/s41590-019-0544-5.

Supplementary information is available for this paper at https://doi.org/10.1038/s41590-019-0544-5.

Correspondence and requests for materials should be addressed to A.K.S. or J.C.L.

Peer review information Laurie A. Dempsey was the primary editor on this article and managed its editorial process and peer review in collaboration with the rest of the editorial team.

Reprints and permissions information is available at www.nature.com/reprints.

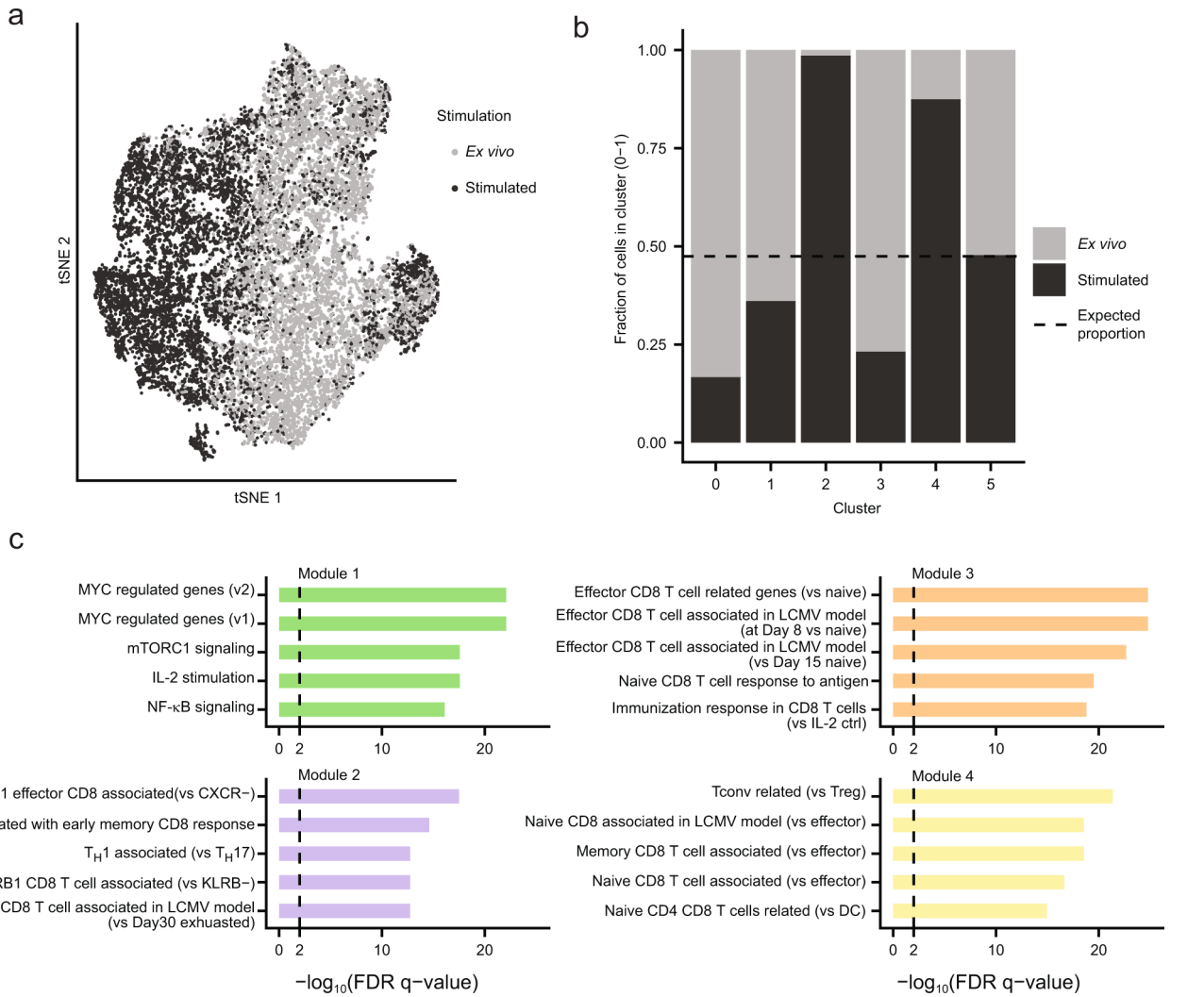

Extended Data Fig. 1 | Stimulated and *ex vivo* cells are transcriptionally distinct. a, tSNE visualization of all cells colored based on stimulation condition (n = 6,912 stimulated cells, dark grey; 7,512 *ex vivo* cells, light grey). **b**, Proportions of stimulated and *ex vivo* cells in each of the computationally determined clusters shown in Fig. 3a. Dash line indicates expected proportions assuming even distributions of cells from both conditions. **c**, Enriched MsigDb signatures of the four modules of genes identified in Fig. 3d. FDR q-values represent Benjamini and Hochberg-corrected, one-tailed hypergeometric *P* values. 50, 49, 35, and 48 genes are included in Module 1, 2, 3, and 4, respectively for enrichment calculation. See Supplementary Table 12 for more details. Data represent combined data from four independent experiments of four mice total (**a-c**).

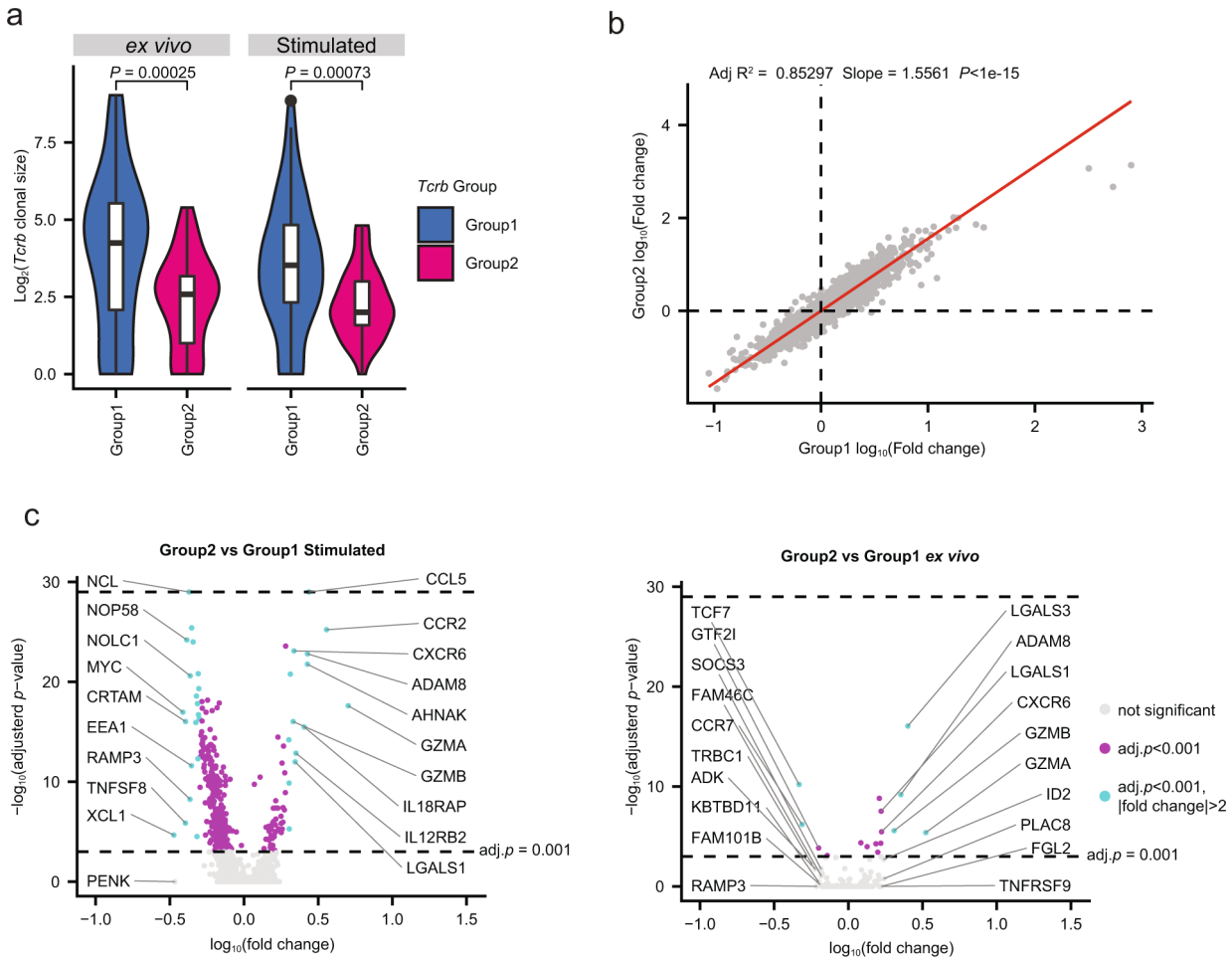

Extended Data Fig. 2 | Group 1 and 2 clonotypes differ in expansion and gene expression upon stimulation. a, Clonal sizes of Group 1 and 2 clonotypes in the stimulated and *ex vivo* conditions shown in Fig. 3d. *P* value calculated by two-sample Mann-Whitney U test (Stimulated: n = 74 clonotype groups in Group 1; 37 Group 2 clonotypes. *ex vivo:* n = 82 Group 1 clonotypes; 40 Group 2 clonotypes). Box and whisker plots indicate the (box) 25th and 75th percentile along with (whisker) +/− 1.5*interquartile range. Violin plots represent estimated density of clonotypes. **b**, Gene expression fold changes between stimulated and *ex vivo* cells in (x-axis) Group 1 clonotypes and (y-axis) Group 2 clonotypes. Each point represents a shared gene across Group 1 and 2 clonotypes. Red line indicates fitted linear model. *P* value calculated by one-tailed *F* statistics (F(1,5908)) of the linear regression. n = 5908 genes. **c**, Volcano plots of differentially expressed genes between Group 1 and 2 clonotypes in the (left) stimulated and the (right) *ex vivo* conditions. *P* values were determined using a two-tailed likelihood ratio test, and adjusted by Bonferroni correction. Top 10 genes with positive or negative fold changes are labeled. Cells in Group 1 and 2 have been downsampled to 300 each (n = 300 cells for each of the groups). See Supplementary Table 13 for more details.

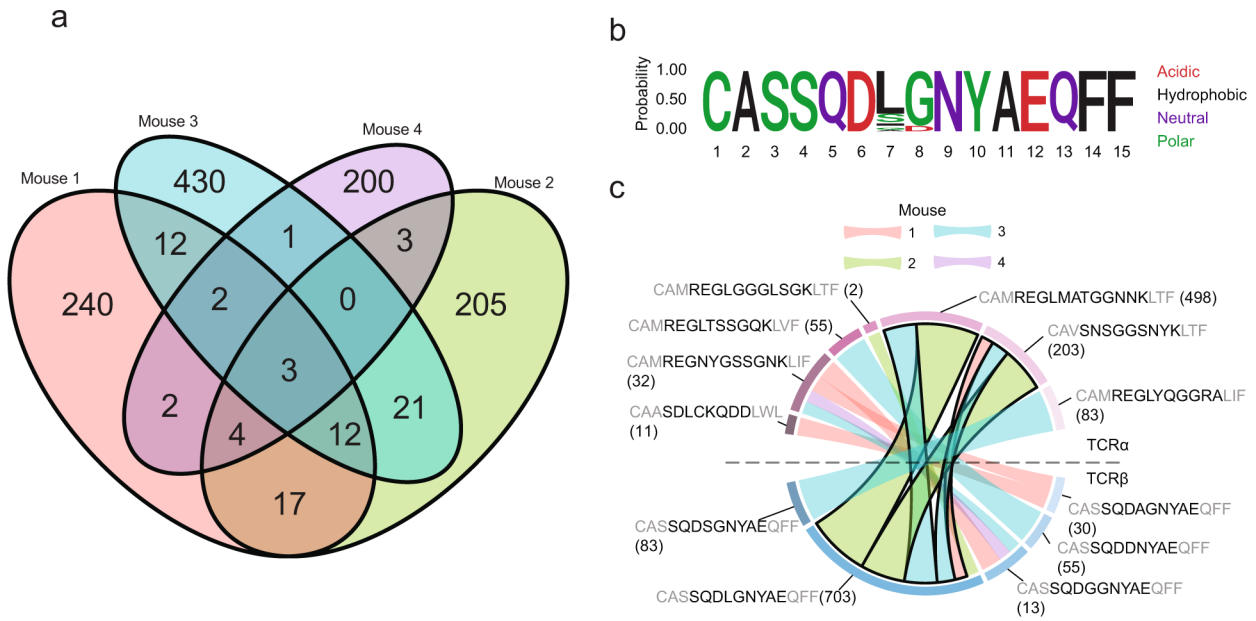

Extended Data Fig. 3 | Analysis of shared clonotypes across four E7-HPV immunized mice. a, Venn diagram of shared unique *Tcrb* clones across the four mice. **b**, Amino acid logo plot of TCRβ sequences that show high similarity among public clones shared by at least three of four animals. Individual sequences are shown in **c**. **c**, TCRα and β matching of highly similar clonotypes found in public clones shared by at least three of four animals (Supplementary Table 9). Bold outline indicates dual TCRα chains found in the same cells (Supplementary Table 3). Structural amino acids shown in grey. Number of cells shown in parenthesis. TCRα and β sequences that were detected in less than two cells were excluded for visualization.

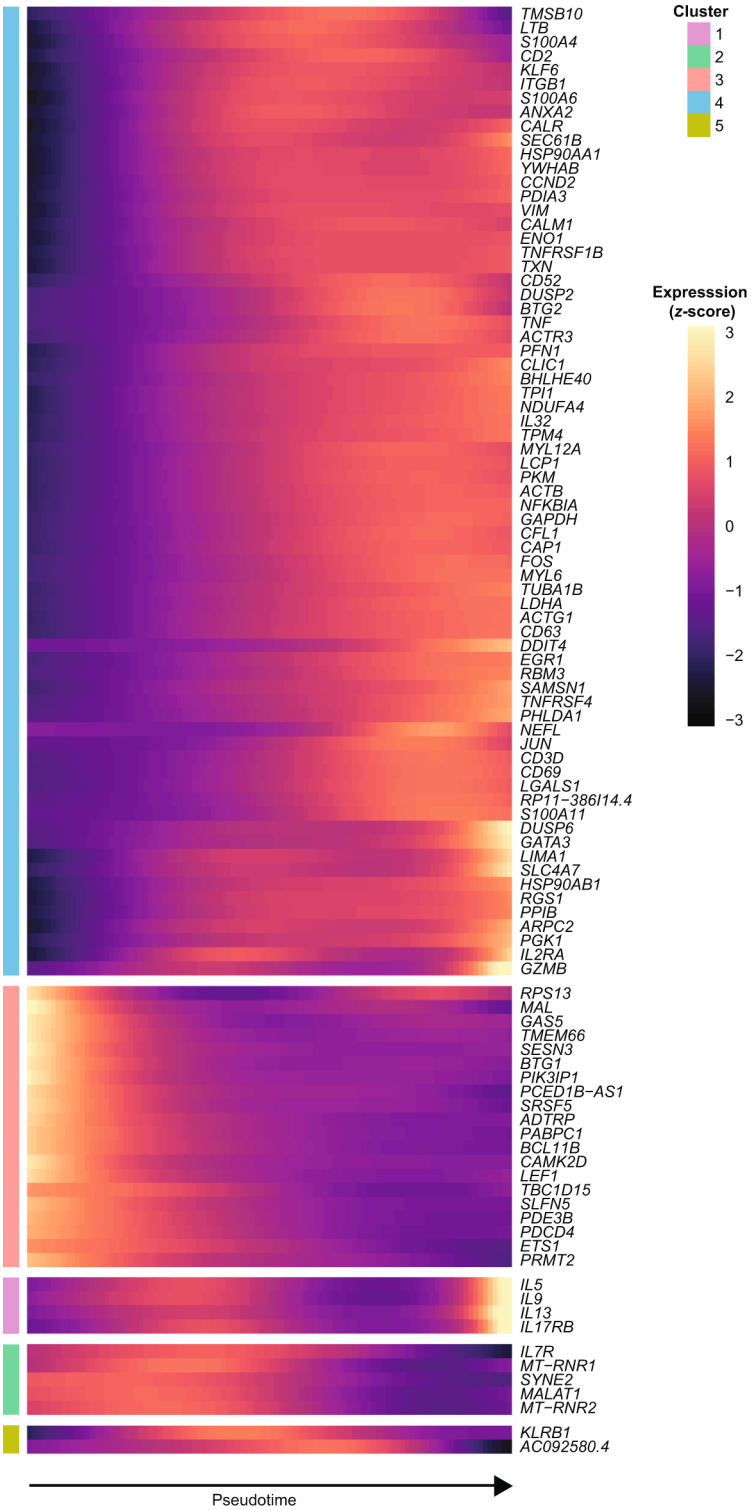

Extended Data Fig. 4 | Distinct patterns of gene expression correlate with pseudotime. a, Expression of top 100 most significant genes visualized across pseudotime. Genes were clustered via Ward.D2 based on their patterns of expression. Data represent an individual experiment with 1847 single-cells from one patient (patient 77).

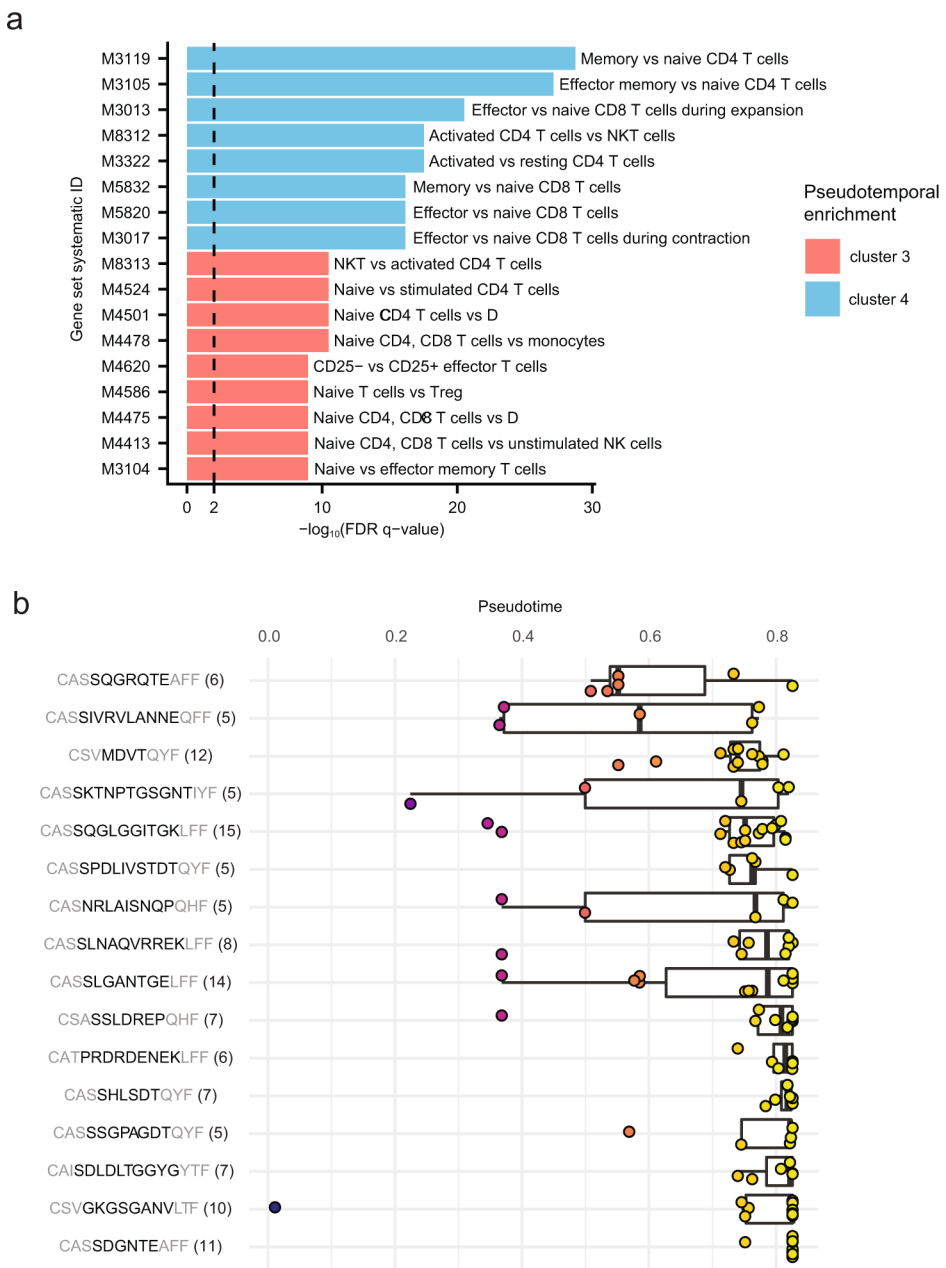

Extended Data Fig. 5 | Psuedotime correlates with effector T cell signatures. a, MsigDB analysis of genes enriched early (cluster 3 in Extended Data Fig 4a; n = 38 genes) or late (cluster 4 in Extended Data Fig 4a; n = 123 genes) on the pseudotemporal trajectory. Description indicates cell state enriched with the corresponding gene set in comparison to another cell state. FDR q-values represent Benjamini and Hochberg-corrected, one-tailed hypergeometric *P* values. See Supplementary Table 12 for more details. **b**, Pseudotime distribution of expanded clones shown in Fig. 4d. Number of cells for each clonotype group indicated in parenthesis. A total of 16 clonotype groups are shown. All box and whisker plots indicate the (box) 25th and 75th percentile along with (whisker) + /− 1.5*interquartile range (**b**). Data represent an individual experiment with 1847 single-cells from one patient (patient 77; **a**,**b**).

nature research

Corresponding author(s): J. Christopher Love and Alex K. Shalek

Last updated by author(s): Oct 17, 2019

Reporting Summary

Nature Research wishes to improve the reproducibility of the work that we publish. This form provides structure for consistency and transparency in reporting. For further information on Nature Research policies, see Authors & Referees and the Editorial Policy Checklist.

Statistics

For all statistical analyses, confirm that the following items are present in the figure legend, table legend, main text, or Methods section.

n/a	Confirmed
☐	☒ The exact sample size (*n*) for each experimental group/condition, given as a discrete number and unit of measurement
☐	☒ A statement on whether measurements were taken from distinct samples or whether the same sample was measured repeatedly
☐	☒ The statistical test(s) used AND whether they are one- or two-sided *Only common tests should be described solely by name; describe more complex techniques in the Methods section.*
☐	☒ A description of all covariates tested
☐	☒ A description of any assumptions or corrections, such as tests of normality and adjustment for multiple comparisons
☐	☒ A full description of the statistical parameters including central tendency (e.g. means) or other basic estimates (e.g. regression coefficient) AND variation (e.g. standard deviation) or associated estimates of uncertainty (e.g. confidence intervals)
☐	☒ For null hypothesis testing, the test statistic (e.g. *F*, *t*, *r*) with confidence intervals, effect sizes, degrees of freedom and *P* value noted *Give P values as exact values whenever suitable.*
☒	☐ For Bayesian analysis, information on the choice of priors and Markov chain Monte Carlo settings
☐	☒ For hierarchical and complex designs, identification of the appropriate level for tests and full reporting of outcomes
☐	☒ Estimates of effect sizes (e.g. Cohen's *d*, Pearson's *r*), indicating how they were calculated

Our web collection on statistics for biologists contains articles on many of the points above.

Software and code

Policy information about availability of computer code

Data collection	Illumina bcl2fastq2.17.1.14 was used to generate fastqs from bcl files. Gene expression data was processed using Drop-seq tools 1.12 (http://mccarrolllab.com/dropseq), and mapped against hg19 or mm9 genome using STAR 2.5.3a then processed using samtools 0.1.19, picard 2.9.0, bwa 0.7.12, Matlab 2016b, and the Matlab Bioinformatics Toolbox 4.10 were used to process TCR sequencing data.
Data analysis	R version > 3.0, Seurat 2.3.4 (and all associated functions), FlowJo v8, Tidyverse, Monocle 3.0 (and all associated functions), MSigDB (http://software.broadinstitute.org/gsea/), viridis, circlize, ggseqlogo, RColorBrewer, and pheatmap were used to analyzed processed TCR and gene expression data. R scripts for generating all analysis, Matlab scripts for processing TCR sequencing data, as well as all updates will be made available on http://shaleklab.com/resources/ or upon request.

For manuscripts utilizing custom algorithms or software that are central to the research but not yet described in published literature, software must be made available to editors/reviewers. We strongly encourage code deposition in a community repository (e.g. GitHub). See the Nature Research guidelines for submitting code & software for further information.

Data

Policy information about availability of data

All manuscripts must include a data availability statement. This statement should provide the following information, where applicable:

- Accession codes, unique identifiers, or web links for publicly available datasets
- A list of figures that have associated raw data
- A description of any restrictions on data availability

FASTQ file format data related to murine samples will be available through GEO and BioProject under accession numbers GSE136028 and PRJNA560970. FASTQ file format data related to human samples will be available through dbGaP under accession number phs001897.v1.p1. Source data files and associated metadata tables for Figures 2-4 will be made available on http://shaleklab.com/resources/, https://github.com/mitlovelab/, or upon request. MsigDB results for Extended Data 1c, Extended Data 5a, and Supplementary Fig. 3h are available as Supplementary Table 12. Full results from differential gene expression comparison shown in Extended Data 2c are available as Supplementary Table 13. All recovered CDR3 sequences, and their frequencies, of TCR alpha and beta chains from E7-immunized mice and

peanut allergy patients are available as Supplementary Tables 6, 10. Gene expression matrices for E7-immunized mice and peanut allergy patients are available as Supplementary Data 1, 2.

Field-specific reporting

Please select the one below that is the best fit for your research. If you are not sure, read the appropriate sections before making your selection.

☒ Life sciences ☐ Behavioural & social sciences ☐ Ecological, evolutionary & environmental sciences

For a reference copy of the document with all sections, see nature.com/documents/nr-reporting-summary-flat.pdf

Life sciences study design

All studies must disclose on these points even when the disclosure is negative.

Sample size	As our study was exploratory and method-centric, we did not predetermine sample size. Given the number of cells we recovered from each Seq-Well chip, we determined that one chip was sufficient for each OT-I spiked-in sample to successfully detect spiked-in cells. Similarly, given the clonal selection of MHC-tetramer reagent and the common genetic background of the mice, we determined that four animals (processed on one Seq-Well chip each) was sufficient to identify common T cell clones across multiple animals. Due to the scarcity of CD154+ T cells in peanut-allergy patients, we included four patients to demonstrate sufficient throughput and recovery of TCR sequences from human samples.
Data exclusions	Described in detail in Methods. Cells were pre-filtered during alignment, and further filtered with no cell accepted with less than 500 genes and 1000 UMIs. TCR data was filtered as described in Methods. UMIs in TCR data with less than 10 reads were filtered. UMIs with no TCR consensus, defined as plurality agreement of sequencing reads attributed to the UMI, were filtered. Filtering criteria were pre-determined before collection of data.
Replication	Reproducibility of the presented method was confirmed using murine samples spiked-in with OT-1 T cells. We detected previously published matching of TCR alpha and beta chains. Furthermore, we performed two technical replicates of the TCR recovery method using the same starting amplified transcriptome libraries. As shown in Supplementary Table 2, the replicates resulted in highly similar data.
Randomization	Randomization was not applicable to the study, as no correlation to outcome was studied.
Blinding	Blinding was not necessary, as no correlation to outcome was studied.

Reporting for specific materials, systems and methods

We require information from authors about some types of materials, experimental systems and methods used in many studies. Here, indicate whether each material, system or method listed is relevant to your study. If you are not sure if a list item applies to your research, read the appropriate section before selecting a response.

Materials & experimental systems

n/a	Involved in the study
☐	☒ Antibodies
☒	☐ Eukaryotic cell lines
☒	☐ Palaeontology
☐	☒ Animals and other organisms
☐	☒ Human research participants
☒	☐ Clinical data

Methods

n/a	Involved in the study
☒	☐ ChIP-seq
☐	☒ Flow cytometry
☒	☐ MRI-based neuroimaging

Antibodies

Antibodies used	The following antibodies were used to identify CD154+ cells from peanut-allergy samples via flow cytometry: Anti-CD154-PE (clone TRAP1; BD Bioscience; dilution 1:5), anti-CD3-AF700 (UCHT1; BD Bioscience; dilution 1:20), anti-CD4-APC-Cy7 (RPA-T4: BD Bioscience; dilution 1:20), anti-CD45RA-FITC (HI100; BD Biosciences; dilution 1:5), anti-CD69-AF647 (FN50; BioLegend; dilution 1:20). The following antibodies were used to identify tetramer positive cells from E7-immunized mice samples via flow cytometry: anti-CD8-APC (clone 53-6.7; BioLegend; 1:100 dilution) and E7-MHC-tetramer-PE (Cat.No.TB-5008-2; MBL; 1:50 dilution).
Validation	All antibodies from BioLegend and BD Bioscience have been individually validated by the manufacturer (data available on respective websites). We also validated the human staining panel by comparing staining of primary human cells after stimulation at different time points to isotype controls and fluorescence minus one controls. CD154 antibody has been described and validated previously in publications such as Chattopadhyay, et al., 2006 Nat Protoc, to identify CD154+ T cells. In the study, the CD154 antibody was compared to isotype controls and used in both antigen-stimulated and ex vivo samples to assess specificity.

E7-MHC-tetramer was validated in Wilmschen, et al., 2018 J. Vis. Exp., to identify antigen-specific T cells. In the study, E7-MHC-tetramer was compared to naive and immunized mice to show specificity. We also validated the mouse CD8 antibody by comparison to isotype control.

Animals and other organisms

Policy information about studies involving animals; ARRIVE guidelines recommended for reporting animal research

Laboratory animals	B6 mice (C57BL/6NTac) were purchased from Taconic. B6 OT-I mice (C57BL/6-Tg) were purchased from Jackson Laboratories. For experiments represented in Figure 2 (and related supplements), all mice were male at age of 8-12 weeks. For experiments represented in Figure 3 (and related supplements), all mice were female at age of 8 weeks at time of immunization.
Wild animals	Study did not involve wild animals.
Field-collected samples	Study did not involve samples collected from the field.
Ethics oversight	All animal work was conducted under the approval of the Massachusetts Institute of Technology (MIT) Division of Comparative Medicine in accordance with federal, state, and local guidelines (CAC protocol #01717-076-20, #0917-092-20).

Note that full information on the approval of the study protocol must also be provided in the manuscript.

Human research participants

Policy information about studies involving human research participants

Population characteristics	All subjects had a previous diagnosis of peanut allergy, a history of peanut-induced reactions consistent with immediate hypersensitivity and confirmatory peanut- and Ara h 2-specific serum IgE concentrations (> 0.35 kU/l; ImmunoCAP; Thermo Fisher).
Recruitment	The human subjects in this study were all screened for participation in a peanut oral immunotherapy trial (NCT01750879) at the Food Allergy Center at Massachusetts General Hospital. The participants all had a previous diagnosis of peanut allergy, a history of peanut-induced reactions consistent with immediate hypersensitivity, and confirmatory peanut- and Ara h 2 (a dominant peanut allergen)-specific serum IgE concentrations (> 0.35 kU/l; ImmunoCAP; Thermo Fisher).
Ethics oversight	All subjects were recruited with informed consent, and the study was approved by the Institutional Review Board of Partners Healthcare (protocol no. 2012P002153) and MIT (protocol no. 1312006071).

Note that full information on the approval of the study protocol must also be provided in the manuscript.

Flow Cytometry

Plots

Confirm that:

☒ The axis labels state the marker and fluorochrome used (e.g. CD4-FITC).

☒ The axis scales are clearly visible. Include numbers along axes only for bottom left plot of group (a 'group' is an analysis of identical markers).

☒ All plots are contour plots with outliers or pseudocolor plots.

☒ A numerical value for number of cells or percentage (with statistics) is provided.

Methodology

Sample preparation	Single-cell suspensions were prepared in FACS Buffer (PBS +1 mM EDTA +25 mM HEPES +1% FBS pH 7.5) before staining for surface antigens. Cells were stained for 30 minutes on ice in FACS buffer and then washed for immediate sorting.
Instrument	FACSAria II instrument (BD Biosciences)
Software	BD FACSDiva Software for collection and FlowJo v8 by TreeStar for analysis
Cell population abundance	Purity of the samples was determined by correlating gene expression results in RNA-Seq to antibody targets in flow cytometry. Minimal number of non-T cells (e.g. monocytes, B cells) were detected (<1%).
Gating strategy	Supplementary Figure 3a and Supplementary Figure 4a for full gating strategy

☒ Tick this box to confirm that a figure exemplifying the gating strategy is provided in the Supplementary Information.